



Airflow design and source control strategies for reducing airborne contaminant exposure in passenger aircraft cabins during the climb leg

Hossam A. Elmaghraby, Yi Wai Chiang & Amir Abbas Aliabadi

To cite this article: Hossam A. Elmaghraby, Yi Wai Chiang & Amir Abbas Aliabadi (2020) Airflow design and source control strategies for reducing airborne contaminant exposure in passenger aircraft cabins during the climb leg, Science and Technology for the Built Environment, 26:7, 901-923, DOI: [10.1080/23744731.2019.1634930](https://doi.org/10.1080/23744731.2019.1634930)

To link to this article: <https://doi.org/10.1080/23744731.2019.1634930>



Accepted author version posted online: 24 Jun 2019.
Published online: 02 Aug 2019.



Submit your article to this journal [↗](#)



Article views: 204



View related articles [↗](#)



View Crossmark data [↗](#)



Citing articles: 1 View citing articles [↗](#)



Airflow design and source control strategies for reducing airborne contaminant exposure in passenger aircraft cabins during the climb leg

HOSSAM A. ELMAGHRABY¹ , YI WAI CHIANG,²  AND AMIR ABBAS ALIABADI^{2*} 

¹Mechanical Engineering Program, University of Guelph, Guelph, Ontario, Canada

²Environmental Engineering Program, University of Guelph, RICH 2515, Guelph, ON N1G 2W1, Canada

The climb leg is one of the most acceleration-intensive periods in a passenger aircraft flight. It was previously found that the passenger exposure to cough-released airborne contaminants during a climb may reach 2.8 to 3.0 times that compared to other legs (Elmaghraby et al., *Science and Technology for the Built Environment*, 2019, accepted. DOI: 10.1080/23744731.2019.1576457). In the current study, airflow design and source control strategies are researched numerically for their ability to reduce cough-released airborne contaminant dispersion in the cabin of a Boeing 767-300 aircraft during a climb. Sulfur hexafluoride (SF₆) was used to mimic the contaminant, which mainly includes cough-released particles in the size range 1.6 to 3 μm in diameter. The airflow design strategies involved altering the supply airflow direction and changing the supply airflow rate. The source control strategies involved changing the cough direction, varying the cough velocity or flow rate, and moving the cougher to different locations in the cabin. Among all cases, relocation of the cougher, changing the airflow direction, and modest increases in airflow rate exhibited the highest reduction in passenger exposure to contaminant compared to the baseline climb case. The exposure reductions were 0.5–0.7 times for the first case, 0.5–0.7 times for the second case, and 0.6–0.7 times for the third case.

Introduction

Air quality and disease transport aboard passenger aircraft have been an intensive research topic in the past few decades, as inferred from a large number of studies in literature (Drake and Johnson 1990; Dechow et al. 1997; Haghghat et al. 1999; Hocking 2000; Nagda and Hodgson 2001; Waters et al. 2002; Lin et al. 2005; Zhang et al. 2009; Poussou et al. 2010; Isukapalli et al. 2013; Li et al. 2016; Yang et al. 2018). This is because the transmission of airborne viruses, such as influenza, tuberculosis, and SARS, is escalated in the closed cabin space through direct passenger-to-passenger exposure and/or from contaminated surfaces (Mangili and Gendreau 2005; European Centre for Disease Prevention and Control 2018). Examples for such transmissions are the in-flight SARS outbreak in China in 2003 and the outbreak of influenza A(H1N1) in 2009, whose

introduction was caused by air travel (Aliabadi et al. 2011). In addition, the complex environment inside passenger aircraft cabins due to the high occupant density and the wide range of passenger activity provides suitable grounds for air quality deterioration and spread of airborne contaminants if no proper remedial measures are taken (ASHRAE 2013; Elmaghraby et al. 2018).

Passenger aircraft perform several flight legs, which are ordered as takeoff, climb, steady level flight (cruise), descent, and landing. During those legs, the aircraft moves at high speeds and experiences various accelerations (Hull 2007). With those accelerations, body forces occur that can significantly affect the airflow patterns and airborne contaminant dispersion within the aircraft cabin. To the authors' knowledge, no previous aircraft ventilation or air quality studies have investigated the effect of such body forces on in-cabin airflow patterns and contaminant dispersion behavior. Rather, studies in the literature have considered that aircraft are stationary or in cruise mode, for which the only applicable body force results from the gravitational acceleration.

However, Elmaghraby et al. (2019) found in a recent study on a Boeing 767-300 aircraft model that among the steady level flight, climb, and descent legs, the climb leg exhibited the highest levels of contaminant surrogate (SF₆) exposures, released from a cough, at two different monitoring locations

Received January 18, 2019; accepted June 13, 2019

Hossam A. Elmaghraby is a PhD Student. **Yi Wai Chiang, PhD, PEng**, is an Assistant Professor. **Amir Abbas Aliabadi, PhD, PEng**, is an Assistant Professor.

*Corresponding author e-mail: aliabadi@uoguelph.ca

Color versions of one or more of the figures in the article can be found online at www.tandfonline.com/uhvc.

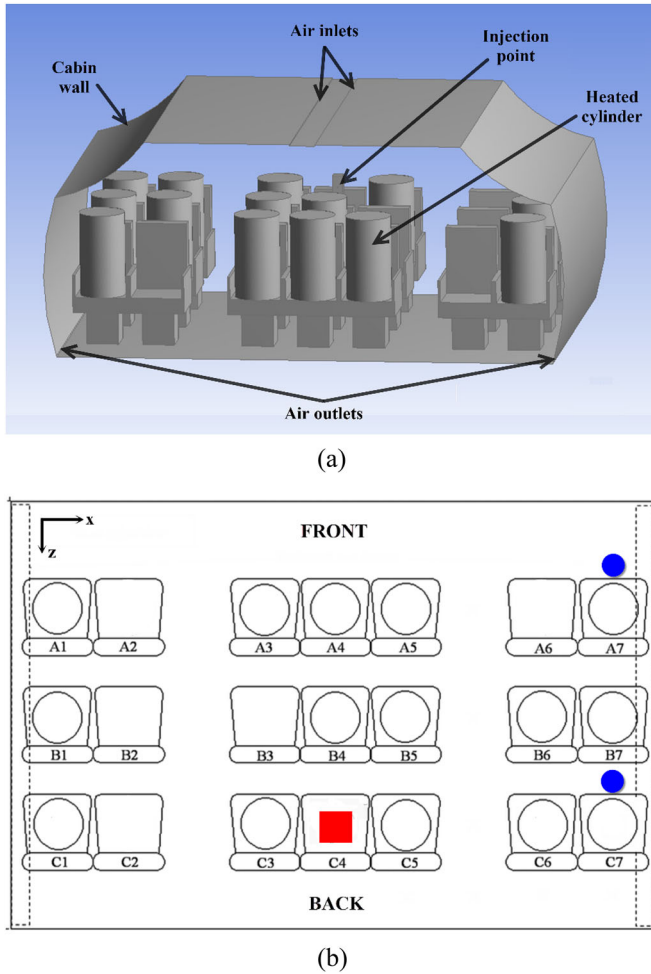


Fig. 1. The Boeing 767-300 cabin model used in the current study. a. Isometric view of the geometry built in ANSYS. b. Plan view for the seats with the cougher/injector position (red square) and the contaminant concentration monitoring points (blue circles). From Elmaghraby et al. (2019).

in the cabin. In addition, variations in airflow patterns and air-flow circulation (r) from one flight leg to the other were noticed. This indicates that acceleration-induced body forces on aircraft have a significant influence on both airflow patterns and contaminant dispersion in the cabin and require further investigation, especially in the form of parametric variations and finding possible means of mitigation (Elmaghraby et al. 2019).

In the current study, different airflow design and source control strategies are investigated as mitigation or reduction means for the increased cough-released contaminant exposure in a passenger aircraft cabin during the climb leg using numerical simulations. The case for the descent leg was not studied due to the evidence that contaminant exposure is not significantly influenced for those legs (Elmaghraby et al. 2019). Airflow design strategies such as changing airflow supply direction and altering airflow rate are employed. The source control strategies considered are changing the cough (or contaminant release) direction, varying the cough velocity/volumetric flow rate, and moving the cougher to other locations in the cabin. Additionally, a continuous mouth-

breathing scheme is employed in the cabin instead of the cough. Lastly, cough-released particles of different sizes are investigated for their dispersion behavior in the cabin during the climb and steady flight legs.

Methods

Cabin model geometry

The aircraft cabin model designed and built in the previous study (Elmaghraby et al. 2019) was based on adopted measurements from two studies in literature: an experimental study by Sze To et al. (2009) and a computational fluid dynamics (CFD) simulation study by Wan et al. (2009) that followed. The original cabin mock-up replicates a full-size sectional economy-class cabin of a Boeing 767-300 passenger aircraft that has 21 seats arranged in three rows. The dimensions of the cabin mock-up are $4.9 \text{ m} \times 3.2 \text{ m} \times 2.1 \text{ m}$ (W, L, H). The cabin mock-up is located at the International Centre for Indoor Environment and Energy, Technical University of Denmark, Lyngby, Denmark (Strøm-Tejsten et al. 2007). For more details about the cabin mock-up's configuration and control systems, the original study by Strøm-Tejsten et al. (2007) can be consulted. In addition, detailed information about the experimental work performed on the dispersion and deposition of expiratory particles in the aircraft cabin mock-up can be found in Sze To et al. (2009) and Elmaghraby et al. (2019). Figure 1 depicts the isometric view (DesignModeler software in the ANSYS 17.0 CFD package) and a plan view for the aircraft cabin model.

Governing Equations

The governing equations solved in ANSYS FLUENT 18.2 and 19.1 for the current model are detailed in the previous study by Elmaghraby et al. (2019) and are summarized here:

- *The mass conservation (continuity) equation:*

$$\frac{\partial \rho}{\partial t} + \nabla \cdot (\rho \vec{V}) = 0, \quad (1)$$

where ρ is the in-cabin air density, t is the time, and \vec{V} is the flow velocity vector. Because the density ρ in the model is constant (independent of space and time), except where buoyancy effects are accounted for, the continuity equation simplifies to the kinematic condition that the velocity field should be *solenoidal* or *divergence-free* (Aliabadi 2018),

$$\nabla \cdot (\vec{V}) = 0. \quad (2)$$

- *The momentum conservation equation:*

$$\frac{\partial}{\partial t} (\rho \vec{V}) + \nabla \cdot (\rho \vec{V} \vec{V}) = -\nabla p + \nabla \cdot (\bar{\tau}) + \rho \vec{g} + \rho \vec{a}, \quad (3)$$

where p is static pressure, $\bar{\tau}$ is the stress tensor, and \vec{g} and \vec{a} are the gravitational and external body accelerations, respectively (ANSYS Inc. 2015).

- *The energy equation:*

$$\begin{aligned} \frac{\partial}{\partial t} (\rho E) + \nabla \cdot (\vec{V} (\rho E + p)) \\ = \nabla \cdot \left(k_{\text{eff}} \nabla T - \sum_j h_j \vec{J}_j + (\bar{\tau}_{\text{eff}} \cdot \vec{V}) \right) + S_h, \end{aligned} \quad (4)$$

Table 1. Boundary and initial conditions for the model.

Boundary and initial conditions	Value
Supply air temperature	24 °C
Supply airflow rate	200 L s ⁻¹ (corresponds to a supply velocity of 2.61 m s ⁻¹)
Supply air absolute humidity	0.92 g kg ⁻¹ (corresponds to 5% relative humidity at supply air temperature)
Cabin wall temperature	18 °C
Heating cylinder heat release	60 W per cylinder (person)
SF ₆ (cough) release location	Seat C4
Air velocity at release location	10.6 m s ⁻¹

where k_{eff} is the effective conductivity = $k + k_t$ (k_t is the turbulent thermal conductivity), T is the temperature, \vec{J}_j is the diffusion flux of species j , and S_h is an additional volumetric heat source (e.g., passenger bodies). E is defined as

$$E = h - \frac{p}{\rho} + \frac{V^2}{2}, \quad (5)$$

where h is the sensible enthalpy of the fluid flow, which is defined for ideal gases (i.e., air) as $h = \sum_j Y_j h_j$, where Y_j is the mass fraction of species j and

$$h_j = \int_{T_{\text{ref}}}^T C_{p,j} dT. \quad (6)$$

For the pressure solver used, T_{ref} is taken as 298.15 K (ANSYS Inc. 2015).

- *Species transport equation:*

$$\frac{\partial}{\partial t}(\rho Y_i) + \nabla \cdot (\rho \vec{V} Y_i) = -\nabla \cdot \vec{J}_i + S_i, \quad (7)$$

where Y_i is the local mass fraction of each species i in the domain, and S_i is the rate of creation (or consumption) of species by addition (or removal) from the dispersed phase plus any user-defined sources. \vec{J}_i is the diffusion flux of species i , which for mass diffusion in turbulent flows is defined as

$$\vec{J}_i = -\left(\rho D_{i,m} + \frac{\mu_t}{Sc_t}\right) \nabla Y_i - D_{T,i} \frac{\nabla T}{T}, \quad (8)$$

where $D_{i,m}$ is the mass diffusion coefficient for species i in the mixture, $D_{T,i}$ is the thermal (Soret) diffusion coefficient, μ_t is the turbulent viscosity, and Sc_t is the turbulent Schmidt number.

- *Turbulence kinetic energy (k) and turbulence kinetic energy dissipation rate (ε) equations (RNG k - ε model):*

$$\frac{\partial}{\partial t}(\rho k) + \frac{\partial}{\partial x_i}(\rho k u_i) = \frac{\partial}{\partial x_j} \left(\alpha_k \mu_{\text{eff}} \frac{\partial k}{\partial x_j} \right) + G_k + G_b - \rho \varepsilon + S_k, \quad (9)$$

and

$$\frac{\partial}{\partial t}(\rho \varepsilon) + \frac{\partial}{\partial x_i}(\rho \varepsilon u_i) = \frac{\partial}{\partial x_j} \left(\alpha_\varepsilon \mu_{\text{eff}} \frac{\partial \varepsilon}{\partial x_j} \right) + C_{1\varepsilon} \frac{\varepsilon}{k} (G_k + C_{3\varepsilon} G_b) - C_{2\varepsilon} \rho \frac{\varepsilon^2}{k} - R_\varepsilon + S_\varepsilon, \quad (10)$$

where α_k and α_ε are the inverse effective Prandtl numbers for k and ε , respectively; S_k and S_ε are user-defined source

(or sink) terms; and $C_{1\varepsilon}$, $C_{2\varepsilon}$, and $C_{3\varepsilon}$ are constants defined by the RNG k - ε model theory. In addition, G_k represents the generation (or consumption) of turbulence kinetic energy due to the mean velocity gradients, and G_b is the generation (or consumption) of turbulence kinetic energy due to buoyancy, which is formulated using the standard gradient diffusion hypothesis as

$$G_b = -g_i \frac{\mu_t}{\rho Pr_t} \frac{\partial \rho}{\partial x_i}, \quad (11)$$

where g_i is the component of the gravitational vector in the i th direction, μ_t is the turbulent viscosity, and Pr_t is the turbulent Prandtl number.

Boundary and initial conditions

The model's boundary and initial conditions in the original studies (Sze To et al. 2009; Wan et al. 2009) were adopted and closely implemented in the numerical solver FLUENT 18.2, and later version 19.1, for the case of 200 L s⁻¹ supply airflow rate through the conventional mixing ventilation system used. Sulfur hexafluoride (SF₆) gas was released in the cabin to mimic the injection and transport of the cough's smallest size droplets (typically 1.6 to 3.0 μm) and that formed the largest number concentration of the injected droplet ensemble in the experiments. The SF₆ was introduced as a surrogate to the smallest size cough particles because of its high density and molecular weight (about 6.14 kg m⁻³ and 146.06 g mol⁻¹, respectively), which make it capable of mimicking the flow behavior of those particles in the cabin (Zhang et al. 2009; Li et al. 2014). This approach was also adopted to reduce the computational burden of simulating particle motion in the model considering that the current model adopts a reductionist approach. Table 1 shows the boundary and initial conditions for the current model.

The simulation was run in two parts. First, the airflow domain was completely solved in the steady mode and then the transient section of the simulation was initiated with the cough (SF₆) release for 1 s with a volume of 0.4 l. After this release was stopped, the transient simulation continued for a total time of 350 s.

The standard wall functions were used for near-wall flow treatment, and the SIMPLE solution algorithm was used for the pressure-velocity coupling. A least squares cell-based method was employed as the spatial discretization scheme gradient, a second-order method was used for solving the

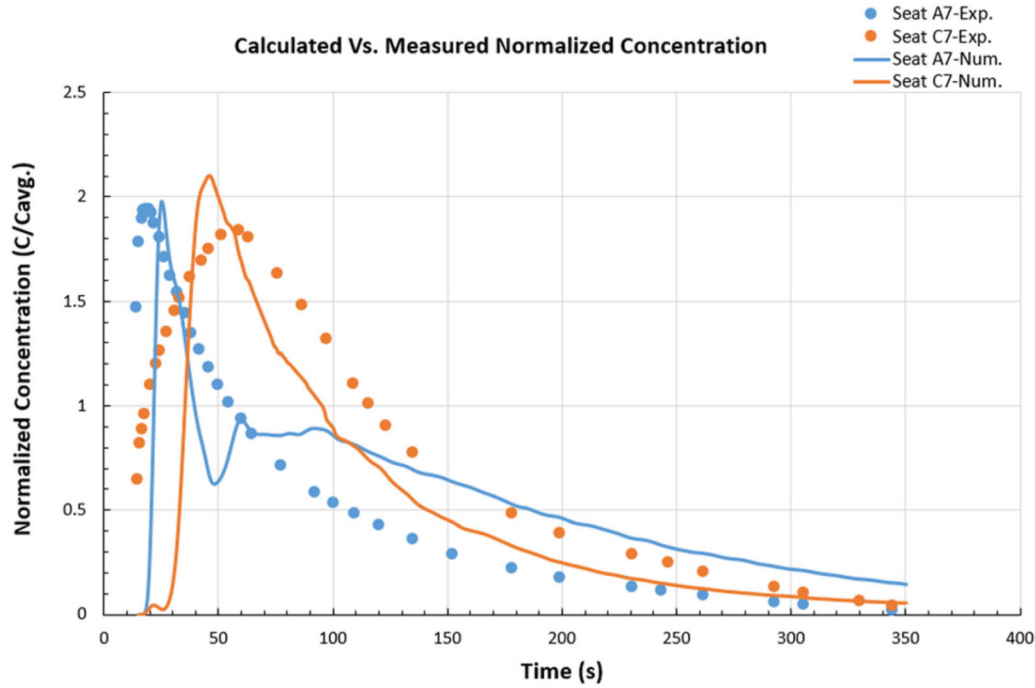
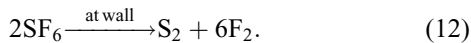


Fig. 2. Comparison of the normalized SF₆ concentration time series between the experimental measurements and numerical calculations using the RNG k - ϵ turbulence model on the fine grid level.

pressure, and a second-order upwind method was used to solve all other equations (momentum, species, turbulence, energy, etc.). For the temporal discretization, however, the first-order implicit method (implicit backward Euler method) was employed for the transient part of the simulation following a fixed time stepping procedure with a time step size of 0.1 s while allowing ten solution iterations per time step.

To accurately simulate cough particle deposition on walls and surfaces, the SF₆ gas was not allowed to bounce off the walls and surfaces in the cabin model. A surface reaction boundary condition at every wall and surface was set to dissociate SF₆ upon contact to its basic gaseous components, sulfide (S₂) and fluorine (F₂) gases, according to the following reaction:



Because the released SF₆ in the cabin was already at very low concentrations, the concentrations of the sulfide and fluorine gases produced from its dissociation were extremely low and did not affect the air composition, fluid properties, or monitored SF₆ concentration in the cabin. This method allows a surrogate simulation of small particles that behave like gases in the aircraft cabin with very economical computation.

Model validation and error estimation

The previous study (Elmaghraby et al. 2019) presented a thorough grid independence analysis of the current model. In addition, it presented model validation through error estimation of the calculated SF₆ concentration time series at the

two monitoring seat locations (seats A7 and C7) using various Reynolds-averaged Navier-Stokes turbulence models (standard k - ϵ , RNG k - ϵ , realizable k - ϵ , standard k - ω , and Shear Stress Transport (SST) k - ω). Thus, the grid independence study will not be repeated here. However, a model validation of the normalized SF₆ concentration time series calculated using the Re-Normalization Group (RNG) k - ϵ model, which was previously found to be the most accurate model, against experimental measurements is shown in Figure 2.

The numerical solution was obtained on a fine grid (7,375,800 grid elements) with the RNG k - ϵ turbulence model that is capable of simulating buoyancy effects on the production and dissipation of turbulence kinetic energy (k).

In previous studies (Aliabadi et al. 2017; Elmaghraby et al. 2019), the error estimation for the model predictions was calculated as the fractional mean bias (FB) and normalized mean square error (NMSE) measures (Hanna 1989). The FB and NMSE are defined as follows:

$$\text{FB} = \frac{2(\overline{C_o} - \overline{C_p})}{(\overline{C_o} + \overline{C_p})} \quad (13)$$

$$\text{NMSE} = \frac{\overline{(C_o - C_p)^2}}{(\overline{C_o} * \overline{C_p})}, \quad (14)$$

where C_o and C_p are the observed (experimental) and predicted (numerical) concentrations, respectively. Whereas FB is a measure of the shift between the observed and predicted quantities, NMSE is a measure of the spread between observed and predicted quantities. For a perfect model, FB

Table 2. FB and NMSE values for the numerical predictions.

Seat	FB	NMSE
A7	0.31867	0.71138
C7	0.39909	0.37711

and NMSE are both equal to zero (Chang and Hanna 2004; Hanna and Chang 2012).

Table 2 provides the FB and NMSE values calculated for the normalized SF₆ concentration time series between the experimental measurements and the numerical predictions of the simulation using the RNG *k-ε* turbulence model.

From Table 2 it can be observed that the NMSE values for normalized SF₆ concentration time series at seat C7 are about 50% less than at seat A7, whereas FB values are almost identical at both seats. This indicates that the shift between the observed and predicted concentration values is similar but the spread of the predicted data with respect to observations is two times higher at seat A7, which indicates less accurate predictions. Physically, this decrease in prediction accuracy can be attributed to the condition of airflow and, consequently, that of the surrogate SF₆ gas from the emission source (at seat C4) to each seat. From C4 to C7 the flow is mainly lateral, which is less susceptible to the bulk flow turbulence than the primarily longitudinal flow experienced from C4 to A7 (see Figure 1).

Calculation of aircraft body acceleration components

The aircraft vertical acceleration (a_v) and horizontal acceleration (a_h) components were calculated during the climb leg using a basic approach adapted from different sources in aircraft dynamics literature (University of Southampton 2005; Gudmundsson 2013; National Aeronautics and Space Administration 2015).

The calculation procedure relies on applying Newton's second law ($\sum \vec{F} = m\vec{a}$) on two axes passing through the center of gravity of the aircraft; one is vertical and the other is horizontal. The forces in action are the lift (L), drag (D), the aircraft's weight (W), and the thrust of the jet engines (T). For example, the relative vertical acceleration on the aircraft cabin during climb was found to be 2.4 *g*, which is composed of two parts; 1.4 *g* due to aircraft acceleration and 1 *g* representing the gravitational component. More information on the calculation procedure followed during the climb leg can be found in the Appendix.

Results and discussion

As highlighted in the Introduction, the SF₆ concentration was found to be the highest at the two monitoring locations considered during the climb leg compared to the steady level flight and descent legs. The calculated SF₆ concentration time series during the three flight legs are graphically shown in Figure 3. In addition, it can be observed from Figure 3 that the SF₆ concentration time series during the descent leg

is similar to that during the steady level flight leg with no significant difference. This can be attributed to the low speed of the passenger aircraft during descent yielding limited acceleration components. Although changing some model factors, such as the location of the cougher (contaminant injector), cough velocity, or airflow conditions, may alter this resemblance between the steady level flight and the descent legs, the large relative difference in SF₆ concentration between the mentioned two legs and the climb leg favors investigation of the climb leg. Therefore, the current study will only consider the climb leg, and different airflow design and source control strategies will be investigated as remedial techniques to the increasing SF₆ concentration noticed during this leg.

In addition to the SF₆ concentration, the exposure of the passengers to SF₆ over time was used as another measure to assess the effect of the acceleration-induced body forces on the contaminant dispersion in the cabin. The exposure is determined by calculating the area under the curve corresponding to each case using the following integral within the simulation time limits:

$$\text{Exposure} = \int_0^{350 \text{ s}} C_{\text{SF}_6}(t) dt. \quad (15)$$

Using this measure, it was found that passenger exposure was always highest during the climb leg when compared to the steady level flight and descent legs. The highest exposure ratio was 3.0 to 1 calculated between climb and descent at seat C7. Nevertheless, the passenger at the same seat experienced a very similar exposure to the contaminant during the descent and steady level flight legs with a ratio of 0.9 to 1 (Elmaghraby et al. 2019).

The approach adopted in the current study for estimating passenger exposure using Equation 15 for calculating the area under the contaminant concentration time series curves was meant to be complementary to the Wells-Riley infection risk assessment model (Riley et al. 1978) widely used in the medical literature.

Infection risk was assessed by the Wells-Riley model using the following equation:

$$P_I = \frac{C}{S} = 1 - \exp\left(-\frac{Iqpt}{Q}\right), \quad (16)$$

where P_I is the probability of infection, C is the number of infection cases, S is the number of susceptible persons, I is the number of infectors, q is the quanta generation rate, p is the pulmonary ventilation rate of a person (or the person's inhalation rate), t is the exposure time interval, and Q is the room ventilation rate with clean air. To accurately predict the risk of infection, many input parameters need to be supplied to the Wells-Riley model. The accuracy and extent of these parameters depend on the desired level of detail for the expected results (Aliabadi et al. 2011).

The Wells-Riley model could not be fully implemented in the model for the current study for two reasons. First, the Wells-Riley model can be only used for the simplified case of a well-mixed room, where the airborne pathogens are uniformly dispersed in the space. This condition was not

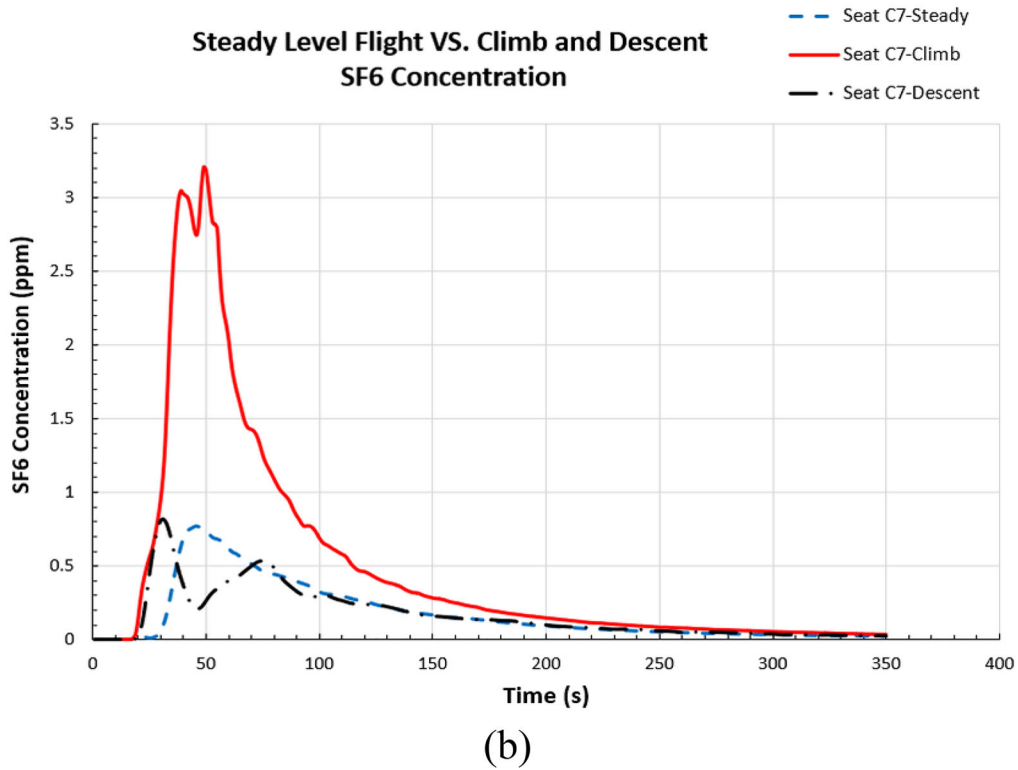
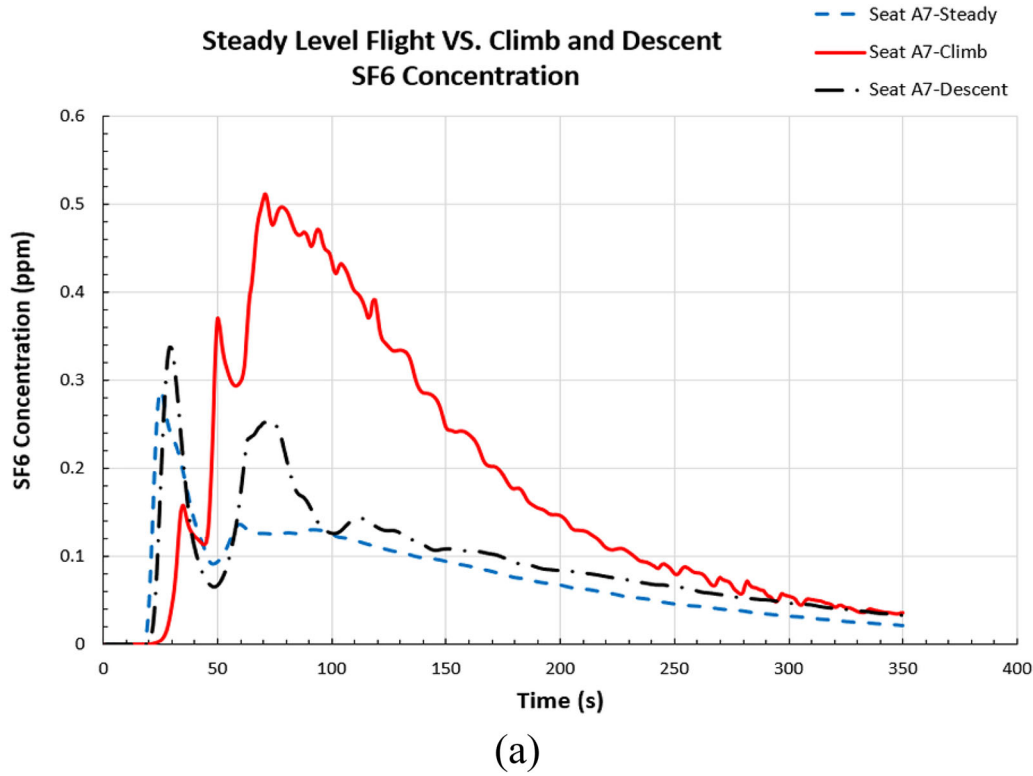


Fig. 3. Comparison of the predicted SF₆ concentration time series among steady level flight, climb, and descent legs. a. At seat A7. b. At seat C7. From Elmaghraby et al. (2019).

satisfied throughout the full simulation time for the current cabin model during the steady level flight leg. In addition, the cabin condition significantly deviated from the well-mixed condition during the climb and descent legs due to

the influence of body forces. Second, the quanta generation rate, q , cannot be calculated directly but is epidemiologically estimated from an outbreak case, where the attack rate of the disease during the outbreak is substituted into P_I (Sze To

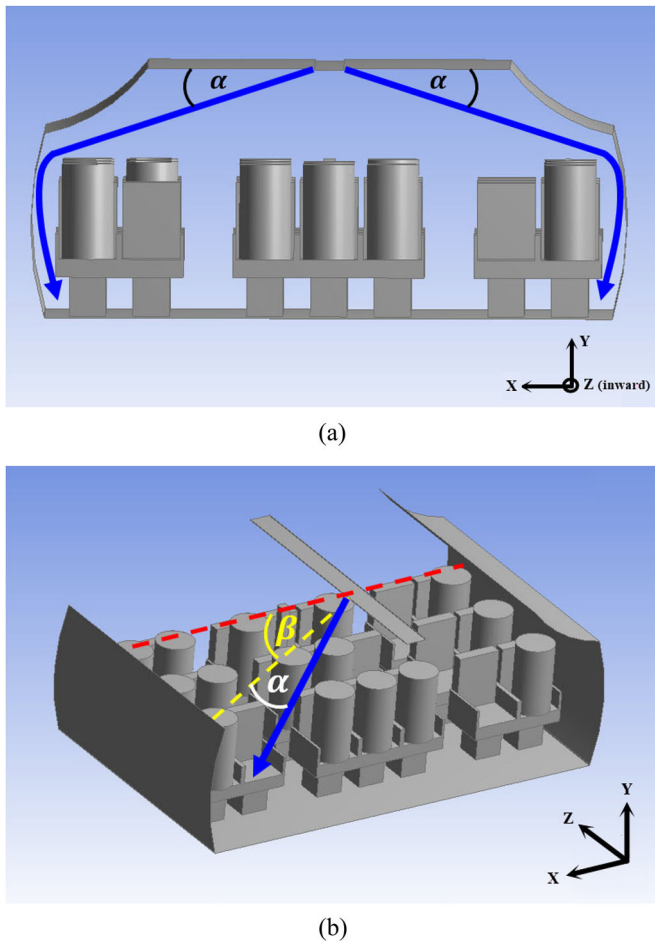


Fig. 4. Redirecting the supplied airflow to the aircraft cabin. a. In 2D using angle α only. b. In 3D using angles α (downwards) and β (front or back) together.

and Chao 2010). Data for an actual outbreak that occurred in the specific cabin configuration/arrangement used in the current study are unavailable. Therefore, the passenger exposure approach was used as an approximate alternative approach to the Wells-Riley model.

Airflow design strategies

Airflow direction

In the current study, the direction of the supply airflow was changed using 2D and 3D approaches. In 2D, the airflow direction was tilted downwards from the cabin ceiling by an angle α . However, in 3D, an angle β was added to direct the airflow either to the front or to the back of the cabin while still being tilted downwards with the angle α . Figure 4 shows examples for using those angles in 2D and 3D views for the cabin model.

Changing angle α only. First, only the change in the supply airflow direction angle α in 2D was considered. Three airflow supply angles were investigated for their ability to reduce the SF₆ concentration exposure in the cabin during the climb leg: 20°, 30°, and 60°. The SF₆ concentration time

series for the 20° and 30° airflow supply scenarios during climb versus that for the standard climb and steady level flight from Elmaghraby et al. (2019) at seats A7 and C7 are shown in Figure 5. However, for readability of the figures, the same comparison for the 60° supply case is shown separately in Figure 6.

From Figures 5 and 6 it can be noticed that there is a considerable difference in the calculated SF₆ concentration time series using each of the three airflow supply angles. The airflow supplied at 30° had the peak SF₆ concentration and, consequently, occupant exposure was reduced to almost 50% of the original concentration during climb at the two monitoring locations. Conversely, the airflow supplied at 20° was not able to provide better air quality conditions at the two monitoring locations, and passenger exposure to the contaminant was almost the same as that for the original climb air supply scenario.

On the other hand, from Figure 6 it can be seen that supplying air at 60° to the cabin produced the worst air quality conditions at the two locations. This is backed by the very high passenger exposure to SF₆ under this air supply condition, especially at seat A7, where the exposure was around 400% of the original case.

To put this comparison in a more graphical way, SF₆ concentration contours are shown in Figure 7 at the breathing level of the occupants during the 30° and 60° airflow supply cases. Due to the transient nature of the simulations, the best representative time window was chosen to show the contours, which is 350 s in this case. As can be seen in the two contour plots, with $\alpha = 60^\circ$ the area covered by the supplied air is very limited at the cabin central area around the two rear seat rows. This leaves most of the seats on the two cabin sides exposed to the contaminant. Conversely, the airflow supplied at 30° efficiently reached the cabin sides and led to reduced passenger exposure at most cabin seats. However, with $\alpha = 30^\circ$, a very minor increase in the SF₆ concentration was seen at the center of the cabin due to the elevated mixing effects induced by the strong airflow eddies at this area.

Changing angles α and β simultaneously. In this alternative airflow redirection approach, angle β is simultaneously changed with angle α to add a 3D perspective to this investigation. Because $\alpha = 30^\circ$ provided the best cabin air quality relative to the other two airflow supply angles in 2D, $\alpha = 30^\circ$ will be used again here with β also chosen to be equal to 30° with supply airflow directed either to the front or to the back of the cabin. This was performed to provide a clear comparison between those two scenarios while limiting the number of simulations required. Figure 8 depicts the SF₆ concentration time series at the two monitoring locations using $\beta = 30^\circ$ to the front and to the back.

Comparing the SF₆ concentration time series at the two locations from Figure 8, it can be seen that the $\beta = 30^\circ$ airflow supply to the back of the cabin could consistently reduce the time-integrated passenger exposure from the original climb case either at seat A7 or seat C7. More specifically, at seat C7, the exposure was reduced to a level close to that for the steady level flight condition. Conversely, in case

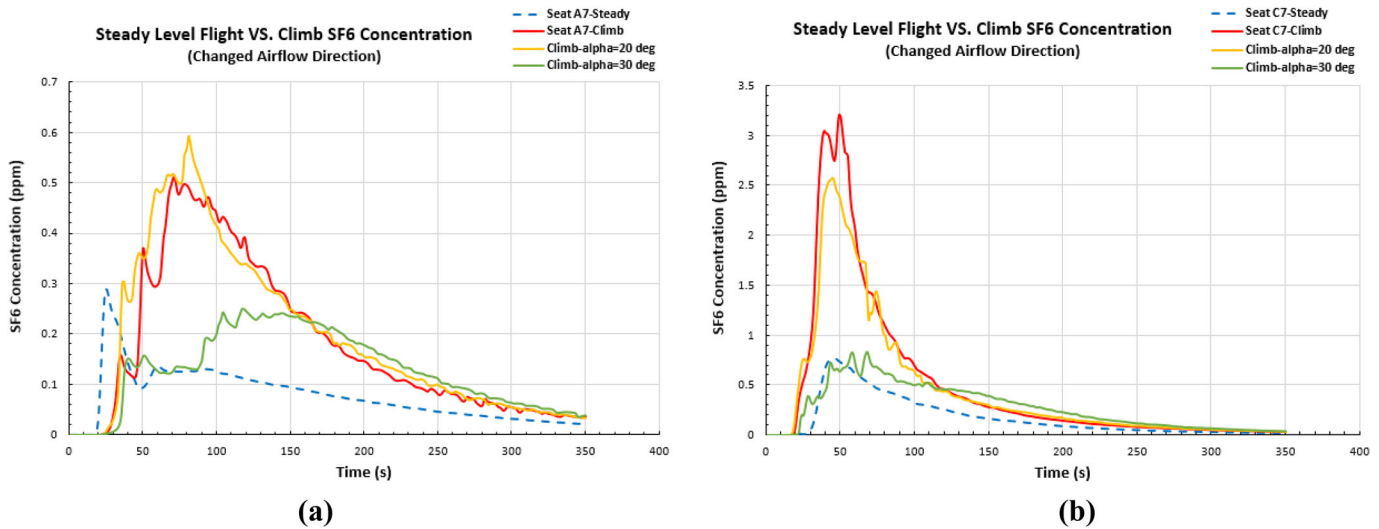


Fig. 5. Comparison of the predicted SF₆ concentration time series between the steady level flight and climb legs using the default, 20°, and 30° airflow supply angles during climb. a. At seat A7. b. At seat C7.

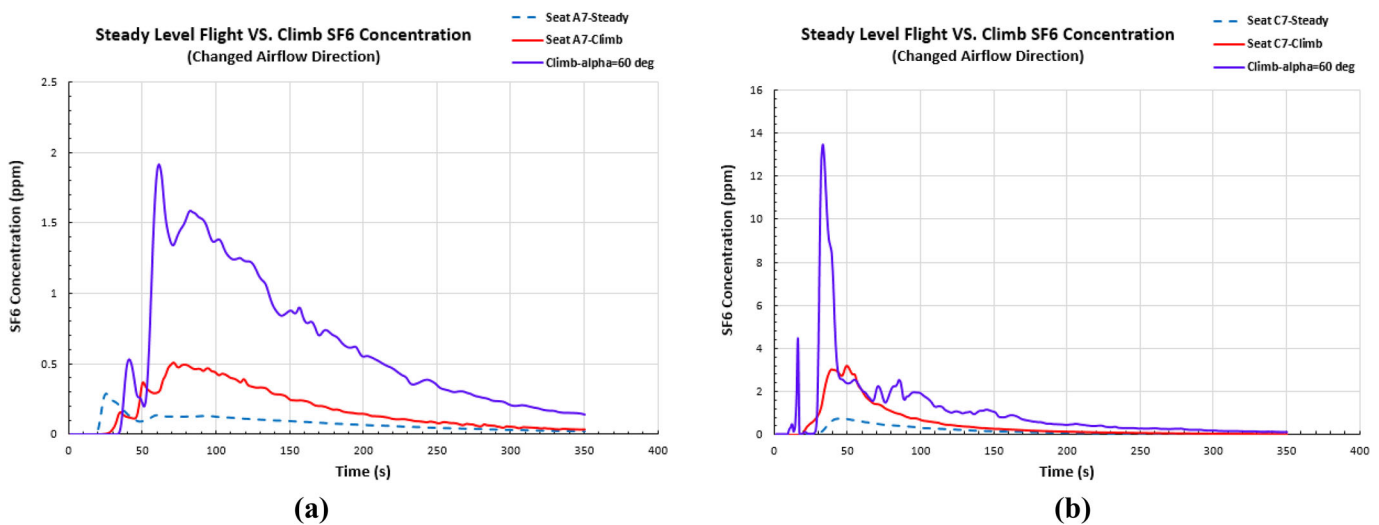


Fig. 6. Comparison of the predicted SF₆ concentration time series between the steady level flight and climb legs using the default and 60° airflow supply angles during climb. a. At seat A7. b. At seat C7.

of the $\beta = 30^\circ$ airflow supply to the front, the passenger exposure was higher at seat A7 than in the original case, but the exposure was almost halved for the same scenario at seat C7. Such a complex response in concentration time series can be understood when the SF₆ contour plots for the mentioned two airflow supply cases at 350 s are compared as shown in Figure 9.

As can be observed from the figure, directing airflow to the front of the cabin pushes the contaminant eventually to the rear of the cabin at the end of simulation time (350 s). Before this happens, however, the air moves most the contaminant to the frontal rows for a short period of time (70–80 s) after contaminant release in the cabin. This explains the very high contaminant concentration at seat A7 around this time. On the other hand, supplying airflow to the back of the cabin leads to steadily pushing the

contaminant to the front of the cabin and providing appropriate dilution of it in the cabin air with no major dispersion patterns in the back rows. This can be attributed to the overall airflow direction being in the same direction of the cough flow in this case. The contaminant dilution provided by the back-directed airflow makes the overall passenger exposure to the contaminant consistently low at most cabin seats, as seen in Figure 9.

Airflow rate

Changing the airflow rate was also investigated as an airflow design strategy to reduce the dispersion of the airborne contaminant in the cabin. The original cabin airflow rate adopted in Elmaghraby et al. (2019) was 200 L s⁻¹ with each of the two inlets providing an equal rate of 100 L s⁻¹. Two cases for airflow rate increase are considered: 100% increase (airflow rate = 400 L s⁻¹) and 50% increase

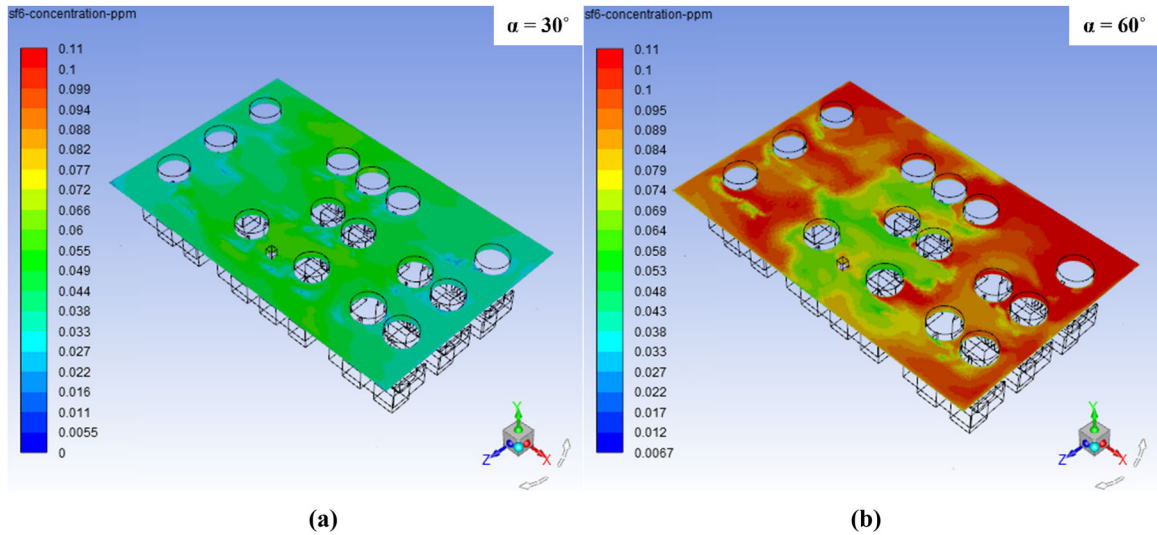


Fig. 7. SF₆ concentration contour plots at passenger breathing level during climb at 350 s. a. Using airflow supply angle $\alpha = 30^\circ$. b. Using airflow supply angle $\alpha = 60^\circ$.

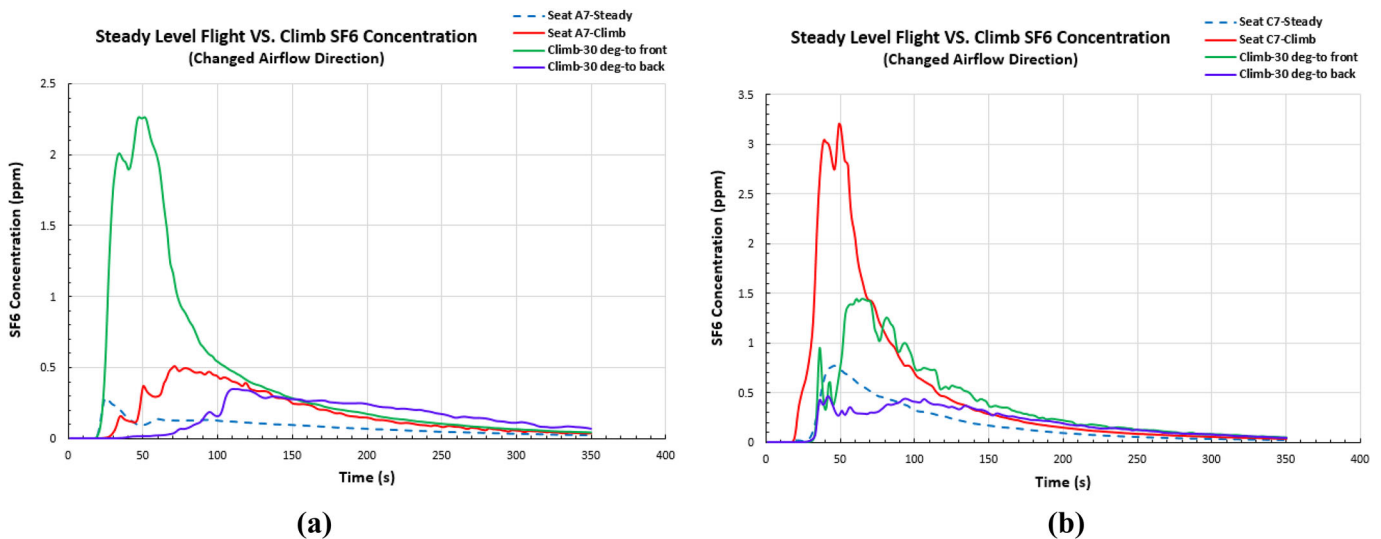


Fig. 8. Comparison of the predicted SF₆ concentration time series between the steady level flight and climb legs using supply angles $\alpha = 30^\circ$ and $\beta = 30^\circ$ (to front and back) during climb. a. At seat A7. b. At seat C7.

(airflow rate = 300 L s^{-1}), and a single case of airflow rate decrease of 50% (airflow rate = 100 L s^{-1}) was investigated. Figure 10 shows a comparison of the three SF₆ concentration time series under the modified airflow rate conditions with the default 200 L s^{-1} case during climb, in addition to the steady level flight case.

As can be noticed from comparing the concentration time series, increasing the base airflow by 100% decreased the passenger exposure to SF₆ at the two monitoring points the most. This was followed by the 50% more airflow rate case, which led to a slightly higher exposure than the previous case. Decreasing the original airflow rate to 50% of its amount led to higher overall exposure at seat A7 and almost the same exposure as the original at seat C7. This latter finding was expected because less airflow means a greater ability of the contaminant to disperse freely in the cabin under

the effect of the cough momentum without a sufficiently large bulk of ventilation air to control it.

However, the 100% more airflow rate case cannot be generally preferred over the 50% more airflow rate based on economic considerations because the former requires more energy consumption, and consequently more fuel utilization, than the latter. In addition, using a higher airflow rate may not always lead to decreased average concentration for an airborne contaminant (Wan et al. 2009; Faulkner et al. 2015), but it could increase the dispersion of such contaminant instead (Sze To et al. 2009). This is especially true for nonuniform contaminant concentrations induced by the complex airflow patterns in an enclosed space (Memarzadeh 2009). Such a condition perfectly describes the dispersion behavior of the cough-released contaminant in the aircraft cabin.

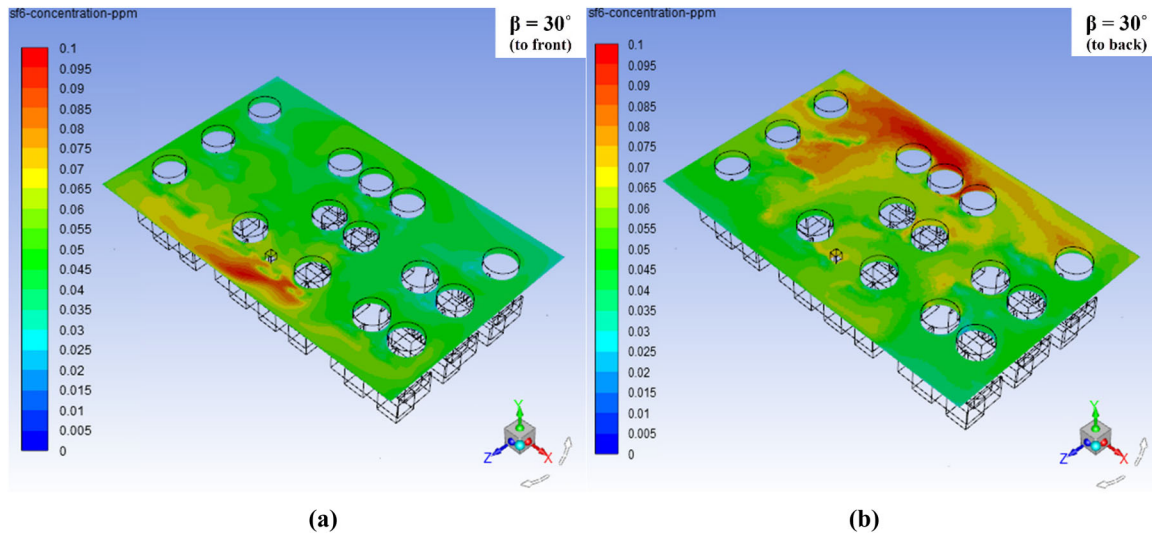


Fig. 9. SF₆ concentration contour plots at passenger breathing level during climb at 350 s. a. Using airflow supply angle $\beta = 30^\circ$ to the front. b. Using airflow supply angle $\beta = 30^\circ$ to the back.

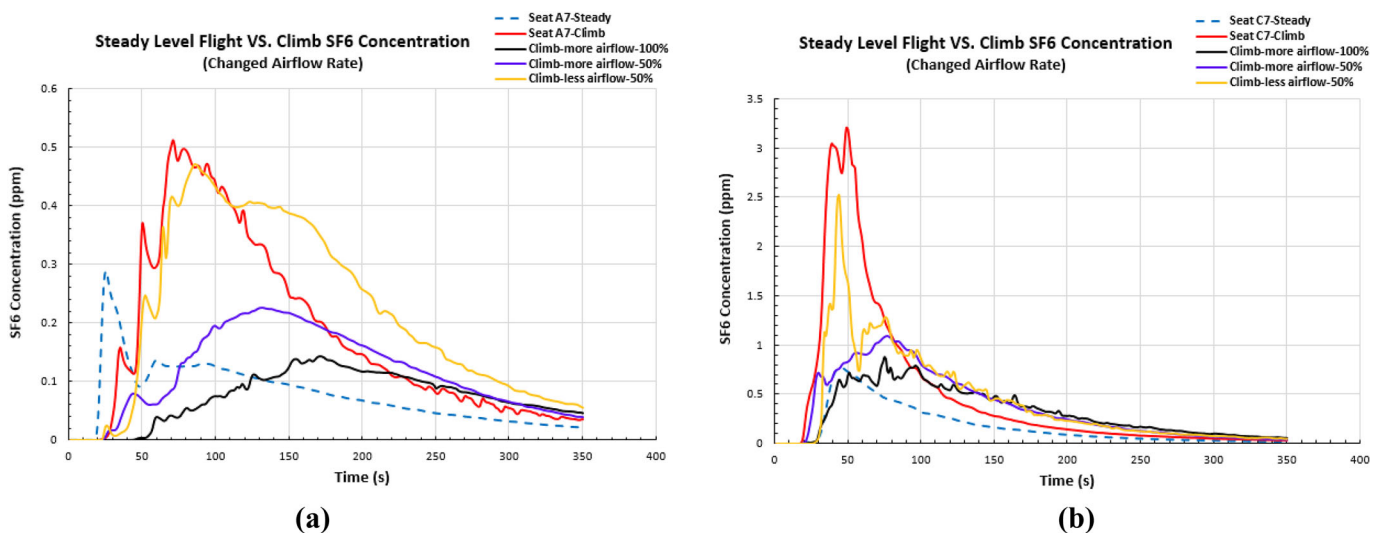


Fig. 10. Comparison of the predicted SF₆ concentration time series between the steady level flight and climb legs using 100% more, 50% more, and 50% less supply airflow rates with respect to the original climb flow rate. a. At seat A7. b. At seat C7.

Figure 11 illustrates the relative dispersion of the contaminant in the cabin at 350 s after release using contours of the three studied cases. From Figure 11 it can be observed that both the 100% more airflow and the 50% less airflow scenarios significantly enhanced the contaminant dispersion in the cabin but using two different mechanisms. Whereas the 100% more airflow case favored a longitudinal dispersion mechanism for the contaminant from the front rows to the back rows of seats, a lateral dispersion mechanism was employed in the 50% less airflow case to mainly move the contaminant from the right side of the cabin to the left side. Those mechanisms can be evidently noticed by combining the SF₆ concentration contour plots with the time series at seats A7 and C7 shown in Figure 10. On the other hand, and although the 50% more airflow case applies a longitudinal dispersion scheme similar to that for the 100% more

airflow case, the former can trap the contaminant at the back of the cabin and reduce its dispersion. This advantage not only significantly decreases the exposure at seats A7 and C7 but also decreases the exposure of the occupants at most cabin seats. This makes the 50% more airflow case superior to the 100% more airflow case.

Source control strategies

Cough direction

Altering the direction of the cough leads to changing the injection orientation for the airborne contaminant in the cabin and can significantly affect its dispersion behavior based on the different surfaces and/or walls the cough stream would encounter with every different orientation. In this investigation, the cough direction was tilted vertically

with specified angles either downwards or upwards from the horizontal but not sideways. This is supported by multiple studies in the literature (Gupta et al. 2009, 2012) that suggest that most of the coughs are directed downwards at the human mouth with two angles ranging from 10° to 20° for the upper angle (between the cough stream and upper lip) and from 36° to 44° for the lower one (between the cough stream and lower lip).

The angles used in this study are 30° and 40° downwards, in addition to 30° upwards. The 30° downwards angle was used as an average of the angles reported by Gupta et al. (2009). However, the other two angles were utilized to investigate the effect of increasing the cough downward tilt angle and the effect of directing the cough upwards on the contaminant dispersion behavior in the cabin, respectively. Figure 12 graphically illustrates the two cough orientations, downwards and upwards, employed in the current investigation. Next, Figure 13 shows the SF₆ concentration time series calculated at the two monitoring positions in the cabin for the three cough direction angles used.

From Figure 13, the calculated concentration time series for the 30° downwards and 40° downwards directions are almost fully coincident. This indicates that increasing or decreasing the cough direction angle for the same cough orientation has no substantial effect on the dispersion pattern of the released contaminant in the cabin. When the cough was directed upwards using $\theta = 30^\circ$, however, the exposure was significantly higher than those for the downwards cough direction. This is because when directed upwards, the cough encounters almost no obstacles that the released contaminant may impact. In addition, in this manner, the contaminant is primarily dispersed from the top of the cabin to the bottom. This significantly enhances the contaminant dispersion aided by the stronger airflow eddies located close to the ceiling due to the thermal plumes created from the bodies of the occupants. Figure 14 clearly shows the difference between the SF₆ contour plots in the cabin at the end of simulation time under the 30° downwards and 30° upwards cough release conditions.

The outcome from the comparison in Figure 14 agrees well with the concentration time series in Figure 13. Releasing a cough with 30° upwards leads to higher concentration of the delivered contaminant at the breathing level of the passengers everywhere in the cabin space, especially in the central region. Such a local increase in the concentration can be attributed to the location of the cougher, which is the middle seat of the back row in this case. However, the cough released by the same person at 30° in the downward direction created a central intensification pattern of the contaminant as well but with much diluted concentrations. These findings can render directing the cough at the release point as an effective source control strategy for the reduction of expiratory airborne contaminants in enclosed spaces such as aircraft cabins.

Cough velocity (volumetric rate)

Another source control strategy investigated in the current study was the cough velocity or volumetric flow rate. Such variances in cough attributes are naturally existent among

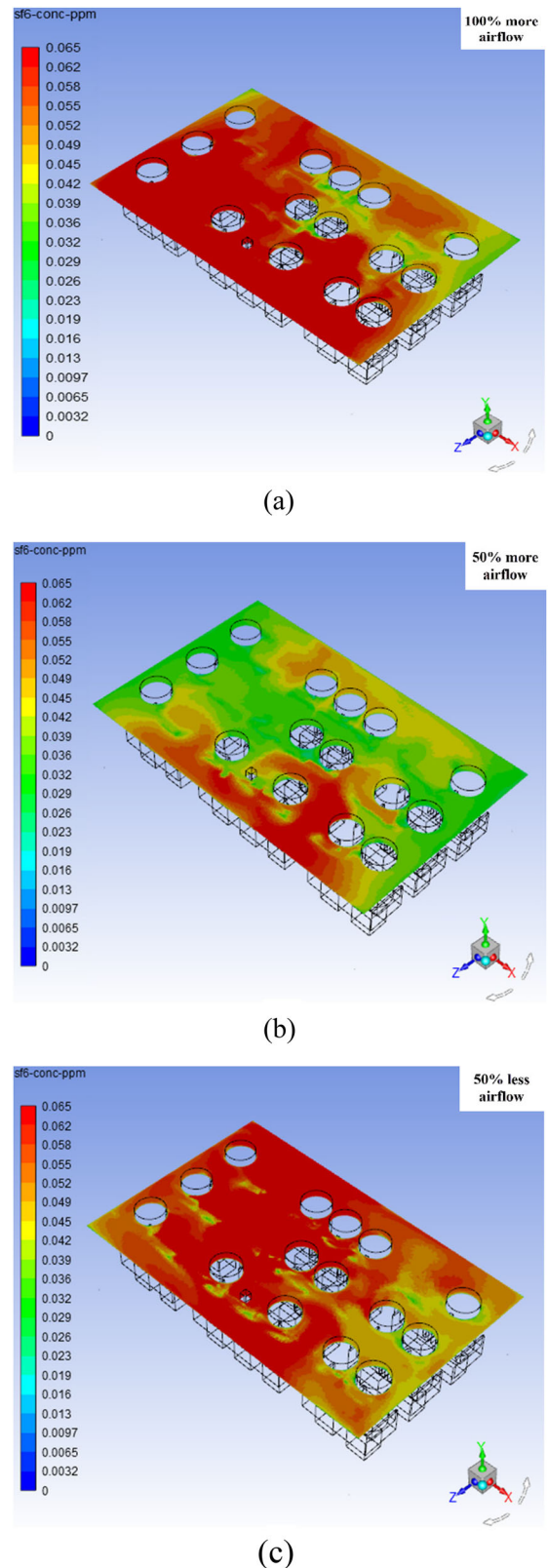


Fig. 11. SF₆ concentration contour plots at passenger breathing level during climb at 350s. a. Using 100% more airflow rate. b. Using 50% more airflow rate. c. Using 50% less airflow rate.

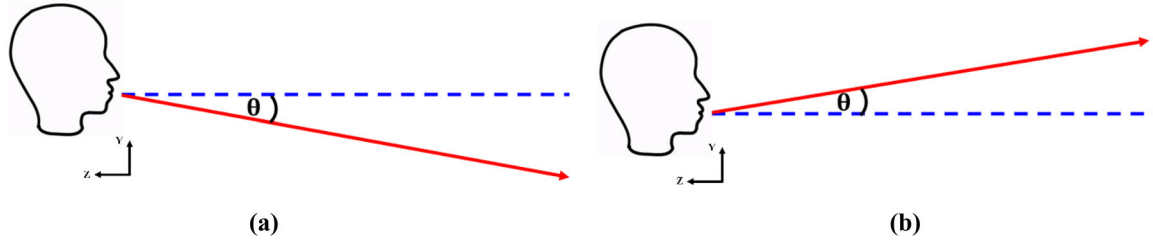


Fig. 12. The two cough orientations used in the current study, where θ is the cough inclination angle. a. Downwards cough. b. Upwards cough.

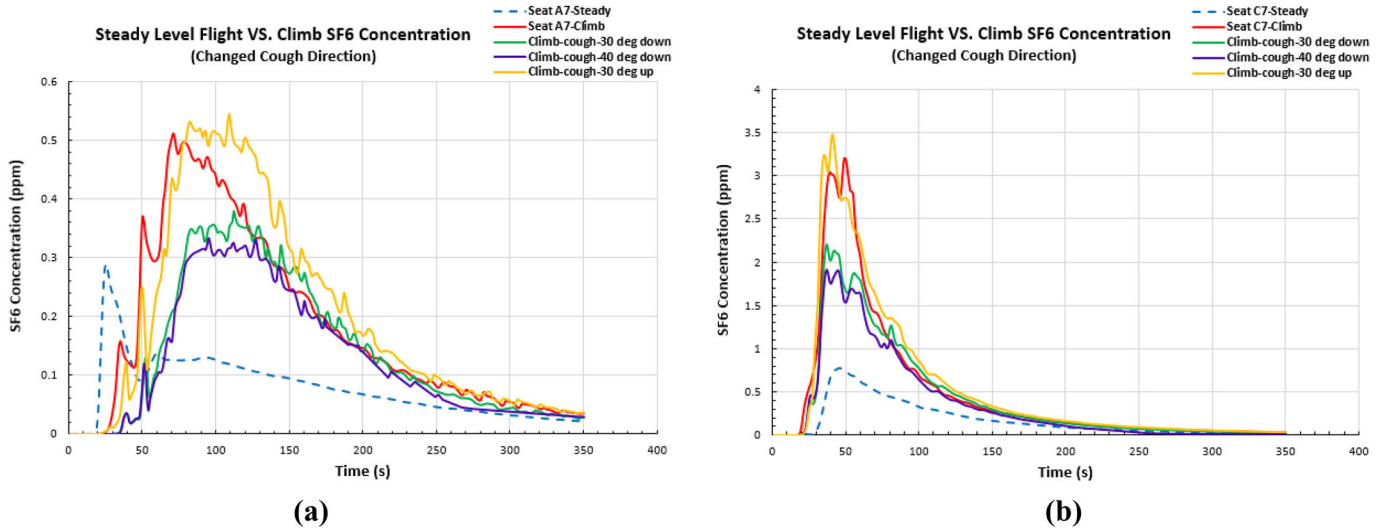


Fig. 13. Comparison of the predicted SF₆ concentration time series between the steady level flight and climb legs using the 30° downwards, 40° downwards, and 30° upwards cough direction angles during climb. a. At seat A7. b. At seat C7.

people of different body sizes, ages, genders, and health conditions. For example, males have a higher cough peak flow rate and cough expiratory volume on average than females. In a sample including 13 males and 12 females, the cough peak flow rate ranged from 3 to 8.5 L s⁻¹ for males and from 1.6 to 6 L s⁻¹ for females, and the cough expiratory volume was anywhere from 400 to 1600 mL for males and 250 to 1250 mL for females, respectively (Gupta et al. 2009).

Additionally, the cough velocity or volumetric rate can be effectively altered at the source using simple habits, such as putting a hand over one’s mouth while coughing or using napkins to obstruct the cough from releasing in the space.

In this study, the investigation of the effect of altering the cough velocity/volumetric rate on the dispersion behavior of the released contaminant in the cabin was conducted using two approaches: variable cough release velocity and fixed-release contaminant mass. The first approach concentrated on changing the cough volumetric flow rate by changing the release velocity of the cough only as the mouth opening area was kept fixed in all cases. The cough velocity was set to two quantities: a low velocity of 5 m s⁻¹ and a high velocity of 20 m s⁻¹ compared to the cough velocity in the previous study (Elmaghraby et al. 2019) of 10.6 m s⁻¹. Alternatively, through the fixed-release SF₆ mass approach, the mass of the injected SF₆ in the cabin was kept fixed between the

new and original cases. This was achieved by changing any two or more variables on the right-hand side of Equation 17 together to keep the contaminant mass (M) on the left-hand side constant:

$$M = C A V T, \tag{17}$$

where C is the contaminant concentration at the release point (mouth), A is the cross-sectional area of the mouth, V is the cough release velocity, and T is the cough time duration. Because C and A are not changed between cases, T is only to be altered with V in an inverse proportional manner. The results for each approach are shown in the following subsections.

Variable cough release velocity. Figure 15 depicts the concentration time series resulting from the high cough release velocity (20 m s⁻¹) and the low cough release velocity (5 m s⁻¹) in comparison to the baseline climb case with 10.6 m s⁻¹ cough velocity and the steady level flight case.

Releasing the cough with a high velocity of 20 m s⁻¹ led to decreased contaminant concentration than the original 10.6 m s⁻¹ and the low-velocity release scenarios for most of the simulation time. This decrease can be attributed to the ability of the higher velocity coughs to quickly disperse in the cabin space, to reach the exhaust slots in considerably less time, and to impact on the cabin envelope compared to the lower velocity coughs.

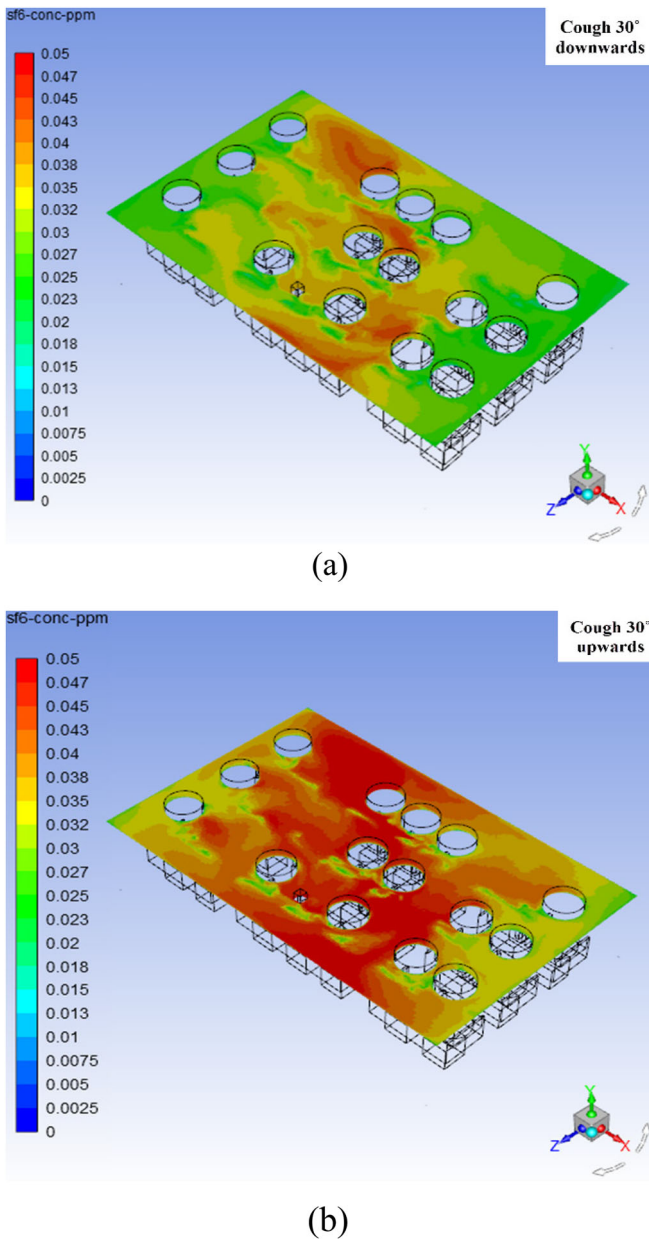


Fig. 14. SF₆ concentration contour plots at passenger breathing level during climb at 350 s. a. Using cough direction angle $\theta = 30^\circ$ downwards. b. Using cough direction angle $\theta = 30^\circ$ upwards.

In this manner, the released contaminant from high-velocity coughs is less likely to settle in a specified location in the cabin for a long time, causing lower local concentrations to be predicted at different locations.

On the other hand, the lower cough release velocity (5 m s^{-1}) results in a contaminant concentration time series that is almost similar to that for the baseline case with a 10.6 m s^{-1} cough velocity. This indicates that as the cough release velocity decreases, the peak local concentration of the released contaminant in the cabin adopts an increasing trend. In addition, the difference between this peak local concentration and that for further lower cough velocities is indistinguishable. Such an increase in peak local contaminant concentration causes higher passenger exposures to the contaminant at different seats.

The cabin-wide contaminant concentration contours under the three cough velocity conditions are shown in Figure 16. It can be noticed that the dispersion pattern of the contaminant in the cabin, especially at the center, is almost identical between the 5 and 20 m s^{-1} cough velocity cases 350 s following the cough release. This good resemblance between the two cases is slightly infracted at the two cabin sides where the contaminant concentration is lower for the 20 m s^{-1} case than for the 5 m s^{-1} case for most of the simulation time. However, starting at around 200 s after cough release, the concentration on the sides is higher for the 20 m s^{-1} case. In contrast, for the 10.6 m s^{-1} cough velocity, the contaminant was further dispersed to the two cabin sides than in the other two cases.

Generally, the three cough release velocity cases showed no clear trend in contaminant dispersion behavior in the cabin, and none of the three cases clearly resulted in a better air quality condition.

Fixed-release SF₆ mass. With an alternative approach, the mass of the released SF₆ from the cough in the cabin, as per Equation 17, was kept fixed. This was attained by doubling the cough release velocity from the baseline case of 10.6 m s^{-1} to 20 m s^{-1} and reducing the cough release duration to 0.5 s instead of 1 s . In this way, the effect of changing the cough release velocity on the released contaminant mass in the cabin could be ruled out. Figure 17 shows the SF₆ concentration time series at the two monitoring locations and the SF₆ contour plots in the cabin for this approach.

From the concentration time series it can be seen that the contaminant concentration at the two measuring points was surprisingly low for the whole simulation time when the cough release velocity was doubled and its duration was halved. Moreover, the contour plots for the same condition show a small concentration as low as 0.004 ppm , which is only about 10% of the average contaminant concentration predicted in the cabin for the 5 and 20 m s^{-1} cough velocity cases in the previous subsection.

Although this approach fixes the released contaminant mass from the cough regardless of the release velocity, the uncommon reduction in the average contaminant concentration in the cabin can be attributed to the weak cough impulse. Despite the increased cough velocity, this weak cough impulse was caused by the significantly decreased cough duration of 0.5 s . This creates a cough that is not fully developed and therefore can be quickly diminished by the strong ventilation air currents in the cabin. Based on these findings, the simulated cough in this case cannot be considered a practical representation of the actual coughs released in the aircraft cabin space. However, if such coughs do exist, they would pose minimal risk to the health of occupants upon exposure.

Cougher location in the cabin

In this investigation, the location of the cougher was changed twice from the back row in the center to the central row on the left side (LC) and to the front row on the right side (RF; looking from the back of the cabin to the front). The new cougher locations with respect to the original case are shown in Figure 18.

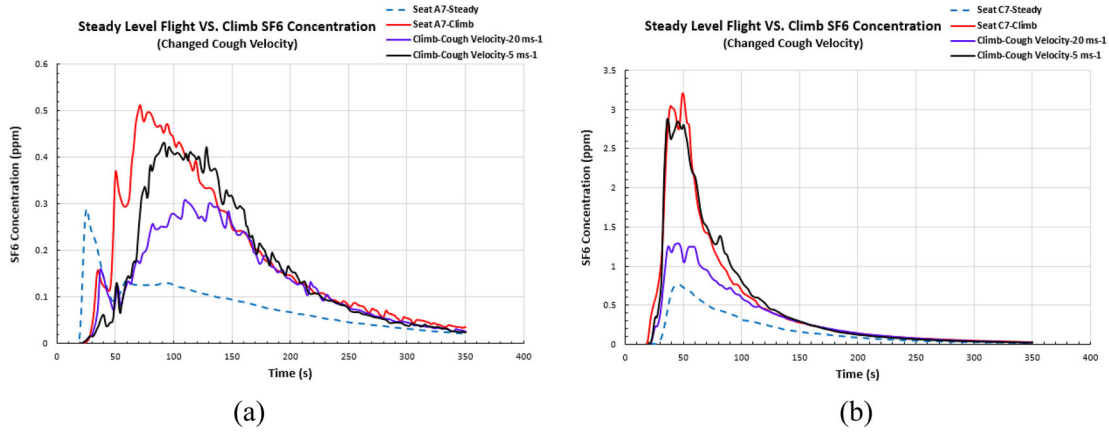


Fig. 15. Comparison of the predicted SF₆ concentration time series between the steady level flight and climb legs using the 20 and 5 m s⁻¹ cough release velocities during climb. a. At seat A7. b. At seat C7.

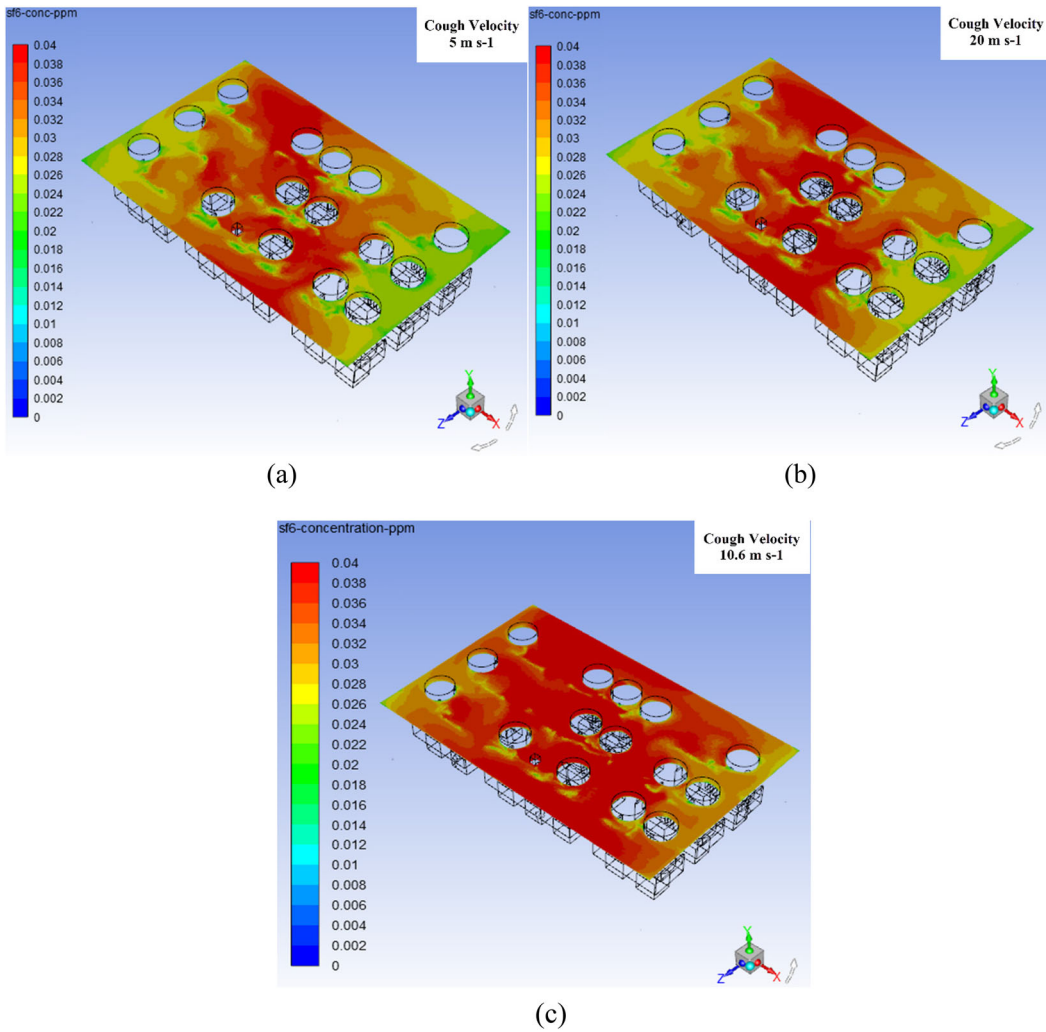


Fig. 16. SF₆ concentration contour plots at passenger breathing level during climb at 350s. a. 5 m s⁻¹ cough velocity. b. 20 m s⁻¹ cough velocity. c. 10.6 m s⁻¹ cough velocity.

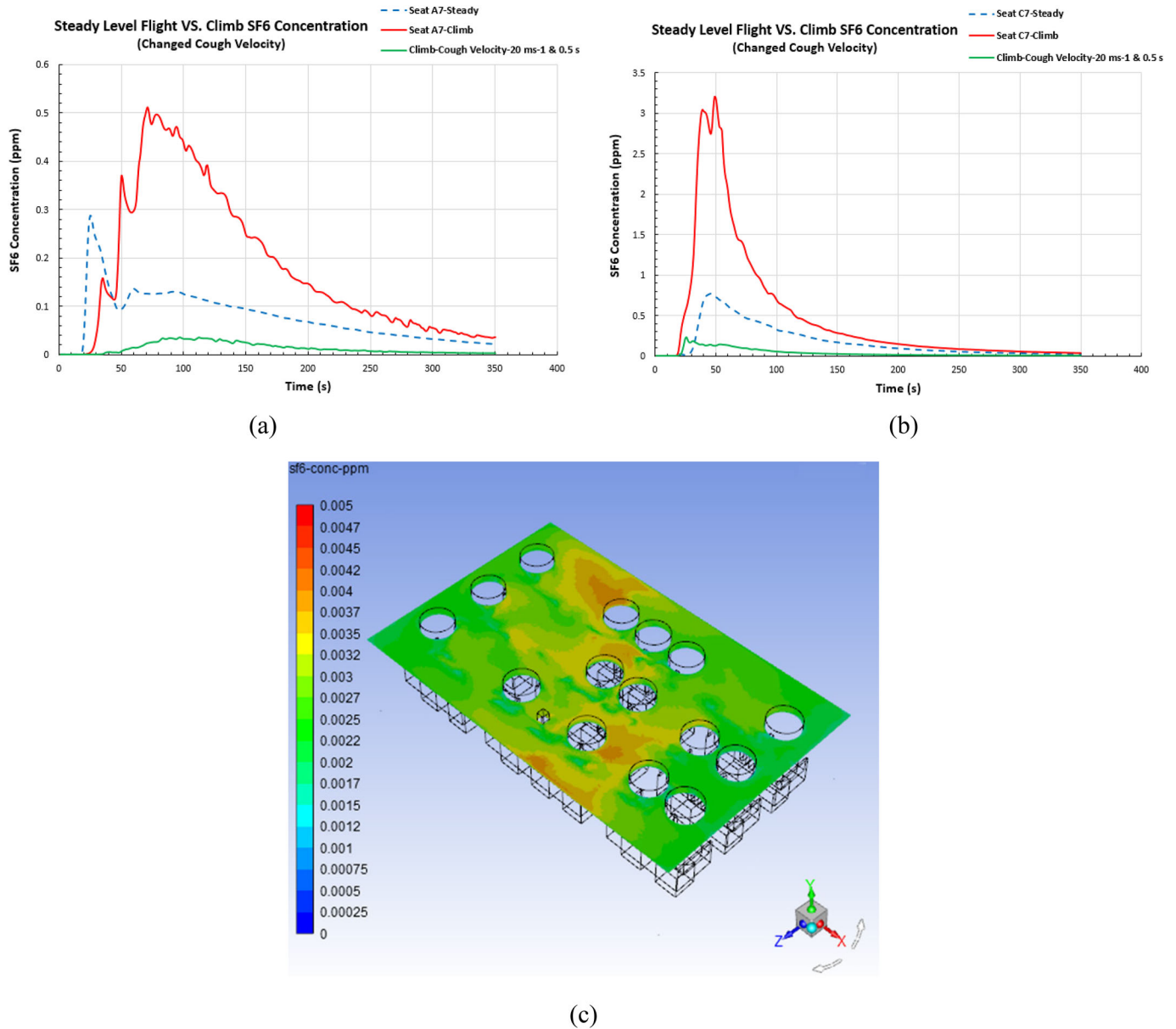


Fig. 17. Predicted SF₆ concentration time series between the steady level flight and climb legs using the 20 m s⁻¹ cough release velocity for 0.5 s during climb. a. At seat A7. b. At seat C7. c. The SF₆ contour plot at passenger breathing level during climb at 350 s for the same case.

Figures 19 and 20 depict the SF₆ concentration time series at the two seats A7 and C7 with the cougher positions at locations LC and RF, respectively. The series for the two cases were separated to enhance their readability.

Based on the concentration time series, the contaminant concentration at each monitoring point was significantly affected by the cougher location. For example, as the cougher moved to the LC location, the concentration at the two monitors for the full simulation time was significantly reduced to a nearly similar level. This is because the cougher at the LC location was almost equally distanced from the two monitoring points. Conversely, because the cougher sitting at the RF location was very close to the monitoring point at seat A7, the contaminant concentration

increased substantially to about eight-fold its maximum value during the baseline climb case, as shown in Figure 20a. On the other hand, at seat C7, the contaminant time-averaged concentration was much lower in the RF cougher location scenario than the baseline case because the cougher was moved further away from it.

In addition to the effect of cougher proximity, the ventilation airflow patterns in the cabin and/or the existence of walls or surfaces close to the cougher location have a significant influence on the dispersion behavior of the released contaminant in the cabin by surface impaction or redirection of the cough. Such an influence can be inferred from the SF₆ concentration contour plots for the two cougher location cases illustrated in Figure 21.

Looking at the contour plot for the LC cougher location, the contaminant was observed to reside at the back of the cabin at the end of simulation. This was impacted by the air-flow in the cabin and the body forces during aircraft climb, which pushed the contaminant to the back rows from the front of the cabin on the left side where it initially dispersed after release. On the other hand, the contaminant released from the cougher in the RF position followed along the frontal cabin separator to the left before it dispersed to the back rows with the aid of airflow mixing. This led to higher concentration regions in the central section of the cabin and greater occupant exposure to the contaminant. According to the results, a coughing person aboard an aircraft may cause a higher probability of exposure not only to the passengers close to him or her but also to most occupants if this person is coughing in proximity to a wall or surface.

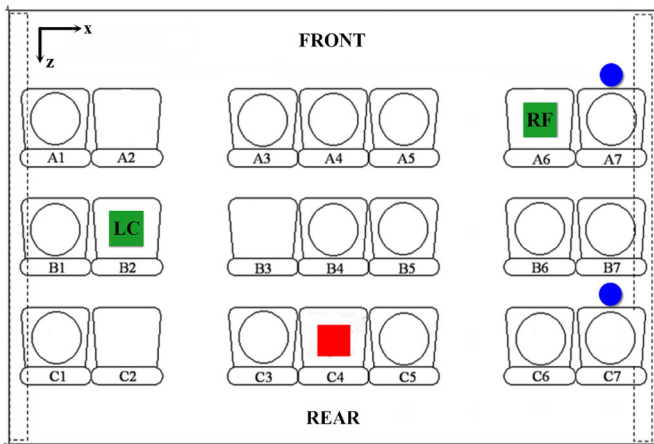


Fig. 18. New cougher locations with respect to the original location (red square). First location is on the left side in the center row (LC) and the second is on the right side in the front row (RF).

Table 3 lists the passenger exposure ratio between the various cases studied in the current article and the baseline climb case.

The exposure values were calculated using Equation 15 and applying the composite Simpson’s and composite trapezoidal rules in determining the area under the curve for each concentration time series.

From Table 3, the lowest average exposure ratio between the two seats was found for the 100% more airflow rate case. The cases that come after the 100% more airflow rate case are the left side, center row relocation of the cougher, the $\alpha = 30^\circ$ airflow direction, and the 50% more airflow rate. For energy saving considerations, however, the latter three cases are preferred over the former one. Such airflow design and/or source control strategies could be implemented to reduce the exposure of aircraft occupants to expiratory contaminants released in this aircraft cabin, especially during the climb leg.

Nevertheless, the highest exposure ratio was noticed for the $\alpha = 60^\circ$ airflow direction scenario. This was followed by the occurrence in which the cougher was moved to the front row on the right side of the cabin and later by setting $\alpha = 30^\circ$ and $\beta = 30^\circ$ to the front as the airflow direction condition.

Continuous breathing

In this section, continuous mouth breathing was investigated as an alternative source of the gaseous contaminant surrogate (SF_6) release to the coughs. Continuous exhalation was only considered from the mouth of the index person (the cougher in previous cases).

The exhalation of other passengers in the cabin was not simulated because the generated thermal plumes from the passengers’ bodies would cause strong turbulence (mixing) effects in the cabin airflow, which significantly surpasses similar effects caused by their low-velocity exhaled air during mouth breathing.

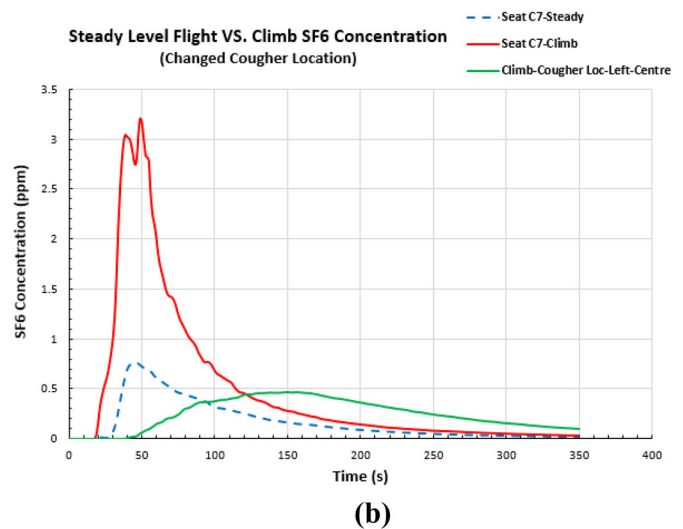
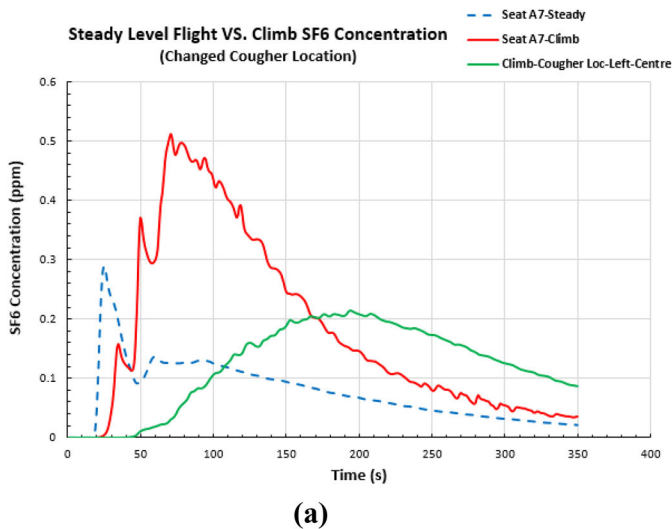


Fig. 19. Comparison of the predicted SF_6 concentration time series between the steady level flight and climb legs with the cougher moved to the center row on the left side of the cabin during climb. a. At seat A7. b. At seat C7.

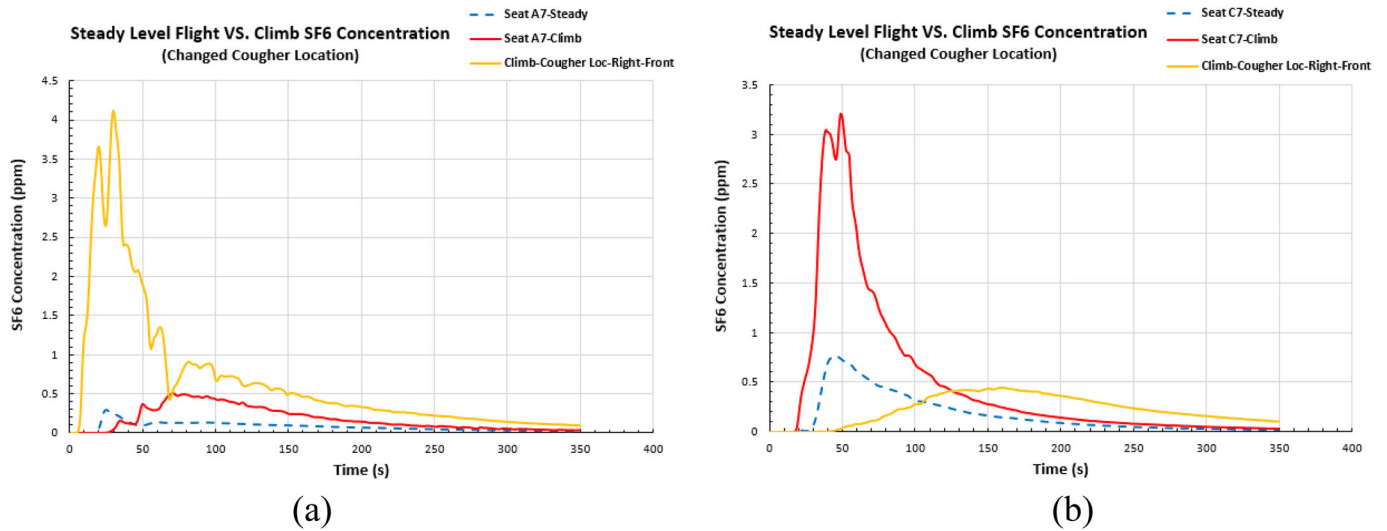


Fig. 20. Comparison of the predicted SF₆ concentration time series between the steady level flight and climb legs with the cougher moved to the front row on the right side of the cabin during climb. a. At seat A7. b. At seat C7.

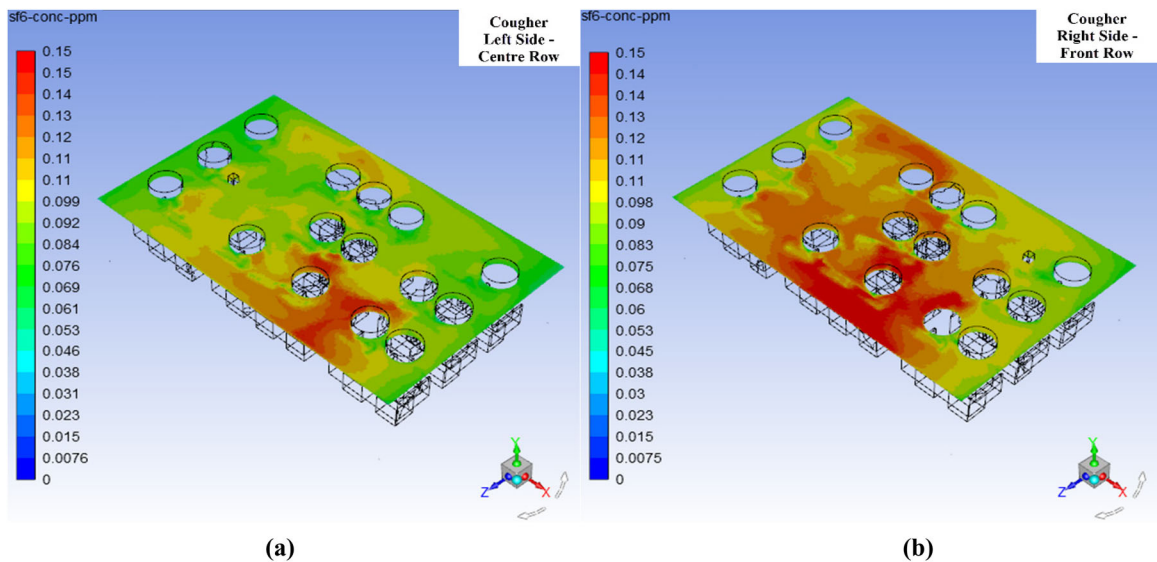


Fig. 21. SF₆ concentration contour plots at passenger breathing level during climb at 350 s. a. Cougher located in the center row on the left side of the cabin. b. Cougher located in the front row on the right side of the cabin.

The exhalation velocity at the index person’s mouth was set at 2 m s^{-1} . This exhalation velocity was defined as an average between the maximum mouth breathing derived velocity measured by Tang et al. (2013); (1.3 m s^{-1}), and the mouth breathing velocity was calculated using the breathing flow rate equations provided by Gupta et al. (2010); (around 3 m s^{-1}). The exhaled air from the occupant’s mouth was assumed to contain a volume fraction of 0.01 (1%) of the SF₆ contaminant mimicking the contagious particles. Figure 22 depicts a comparison of the concentration time series of the released contaminant from the continuous exhalation in the cabin at the two monitoring locations, seat A7 and seat C7, during the steady level flight and climb legs.

From Figure 22, it can be noticed that the concentration of the contaminant at the two monitoring locations in the cabin maintained an increasing trend with the simulation time for both the steady level flight and climb legs. However, this increasing trend tended to plateau near the end of the simulation, more specifically around 250 s since the first release of the SF₆. This implies that even if the simulation were extended beyond the 350 s limit, the contaminant concentration resulting from continuous exhalation would not surpass a specific limiting threshold.

Additionally, for the continuous exhalation case, the concentration of the contaminant was observed to be usually higher during the steady level flight when compared to the

Table 3. Ratio of passenger exposure between different parametric sensitivity cases and the baseline climb case at the two monitoring locations: seat A7 and seat C7.^a

Case	Passenger exposure ratio to baseline climb case	
	Seat A7	Seat C7
$\alpha = 20^\circ$ airflow	1.1:1	0.9:1
$\alpha = 30^\circ$ airflow	0.7:1	0.5:1
$\alpha = 60^\circ$ airflow	3.5:1	2.1:1
$\alpha = 30^\circ$ and $\beta = 30^\circ$ to front	2.4:1	0.7:1
$\alpha = 30^\circ$ and $\beta = 30^\circ$ to back	0.9:1	0.4:1
100% More airflow rate	0.4:1	0.6:1
50% More airflow rate	0.6:1	0.7:1
50% Less airflow rate	1.2:1	0.8:1
Cough 30° downwards	0.8:1	0.8:1
Cough 40° downwards	0.7:1	0.6:1
Cough 30° upwards	1.1:1	1.1:1
Cough velocity 20 m s^{-1}	0.7:1	0.6:1
Cough velocity 5 m s^{-1}	0.9:1	1:1
Cougher at left side, center row	0.7:1	0.5:1
Cougher at right side, front row	3.9:1	0.4:1

Note: ^aThe lowest exposure ratios are presented in bold font.

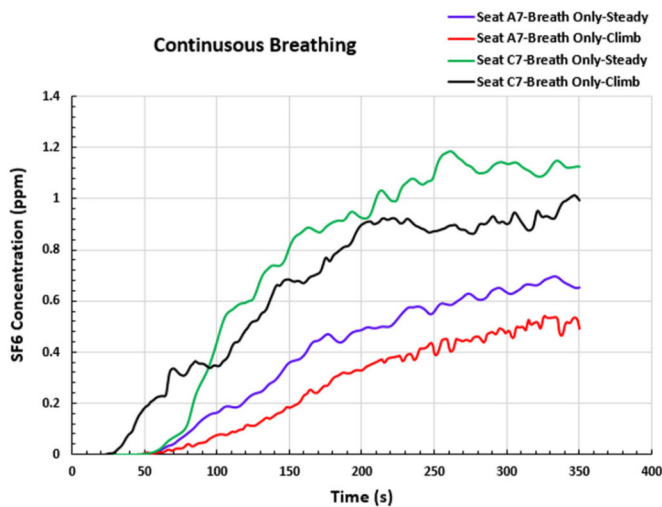


Fig. 22. Comparison of the predicted SF₆ concentration time series resulting from continuous mouth breathing (exhalation only) between the steady level flight and climb legs at the two monitoring locations.

climb leg at the two monitoring locations. Although the concentration during the climb was observed to be higher than that during the steady level flight shortly after the release, especially at the back rows, the latter eventually surpassed the former. Those results, which are contrary to those found for the cough, can be attributed to the different interaction between the continuously released contaminant in the cabin and the background ventilation airflow during the two flight legs. During the steady level flight leg, the contaminant had a greater chance to be distributed evenly in the cabin space aided by the well-mixed cabin condition created by the ventilation airflow. This substantially increased the concentration of the contaminant globally in the cabin. On the other

hand, throughout the climb leg, the released contaminant was pushed to the back of the cabin by the effect of the acceleration-induced body forces. This made the contaminant unable to properly mix with the cabin air, which decreased the overall concentration in the cabin and raised the local concentration at the back row of seats temporarily before the contaminant was pulled out of the cabin from the exhaust grills.

The passenger exposure to the contaminant released from the continuous exhalation in the cabin was estimated at seats A7 and C7 using Equation 15. The passenger exposure between the climb and steady flight legs at seat A7 was 0.7:1, whereas at seat C7 it was 0.9:1.

The findings from this investigation warrant further research on the effect of continuous breathing on the contaminant dispersion behavior in the aircraft cabin under the influence of body forces, which differs from that for the cough.

Cough-released particles

For this investigation, particles of several sizes were used to represent the expiratory contaminant released from the cough instead of the SF₆ gas. This was performed to compare the exposure ratios quantified in Elmaghraby et al. (2019) using the gaseous contaminant at the two monitoring locations in the cabin against that for fine cough particle (<5 μm in diameter) and to extend the study to include coarser particles usually generated from coughs (>5 μm in diameter). Additionally, this follows the theme of several studies in the literature that used particles of different sizes to model expiratory contaminant dispersion from coughing and sneezing (Milton et al. 2013; Tang et al. 2013; Yan et al. 2018). Three particle diameter sizes were utilized in this investigation, namely, 2.5 μm for fine particles and 7.5 and 10 μm for coarse particles.

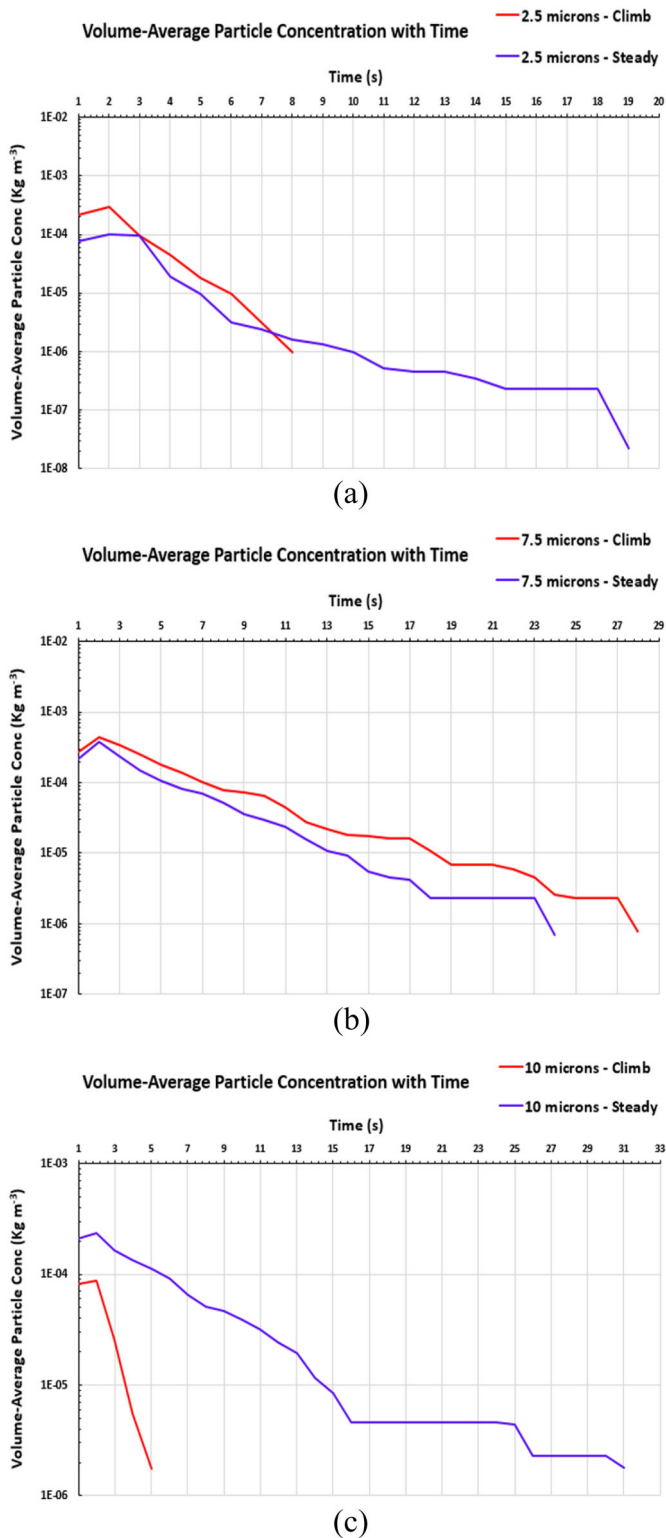


Fig. 23. Comparison of the volume-averaged particle concentration in the cabin with simulation time between the climb and steady level flight legs for three particle sizes. a. 2.5 μm . b. 7.5 μm . c. 10 μm .

Figure 23 shows the concentration of the cough-released particles averaged over the cabin volume (kg m^{-3}) versus the simulation time in seconds for the three investigated particle sizes.

From the figure, it can be noticed that every particle size had a different residence time in the cabin space and that this time was also influenced by the body forces on the aircraft as evident from the dissimilar volume-averaged particle concentration and residence time in the cabin between the climb and steady level flight legs.

Starting with the smallest particle diameter investigated (i.e., 2.5 μm), which represents the fine cough-released particles, the particles remained in the cabin for about 19 s after injection without settling or being trapped on a surface during the steady level flight leg. However, this residence time decreased to 8 s during the climb leg. This difference can be attributed to the ability of those small particles to dilute and further disperse in the cabin during the steady flight leg, whereas they dispersed in the limited cabin rear area only during the climb leg and exited from the domain faster.

Similar behavior was observed for the 10- μm particles, which were the coarsest particles investigated. The 10- μm particles remained in the cabin for longer time (31 s) than the 2.5- μm particles during the steady flight leg due to their greater inertia and slower dispersal rate. However, during the climb leg, the 10- μm particles were faster to settle than the 2.5- μm particles as the body forces moved them to the back section of the cabin where they contacted the walls and surfaces faster due to their larger size.

Conversely, the intermediate particle size of 7.5 μm exhibited a combined characteristic between the 2.5- and 10- μm particles. The 7.5- μm particles remained for 24 s after injection in the cabin during the steady level flight leg, whereas they remained for 28 s during the climb leg. The close residence times between the two legs indicate that the 7.5- μm particles were the least affected with the body forces acting on the aircraft. This also shows that this intermediate airborne particle size can pose the greatest infection risk to passengers because they remain in the cabin for relatively longer times, for almost the whole flight time, regardless of the flight leg.

Table 4 illustrates the ratio of passenger exposure to the different particle sizes between the climb and steady level flight legs taken as an average over the full cabin volume.

From Table 4, the highest passenger exposure ratio between the two legs was observed for the 2.5- μm particles, at 2.2 times during the climb compared to the steady flight, and the lowest was for the 10- μm particles, with a 0.2:1 ratio. However, the 7.5- μm particles had an intermediate exposure ratio of 1.5:1 due to the almost similar dispersion behavior they exhibited between the two legs, as previously mentioned.

Additionally, the exposure ratio for the 2.5- μm particles closely resembled the exposure values previously calculated (Elmaghraby et al. 2019) using the SF₆ expiratory contaminant surrogate at seats A7 and C7 in the cabin, which were 2.4:1 and 2.8:1, respectively. This result suggests that the gaseous contaminant can efficiently mimic the dispersion behavior of the expiratory airborne particles in the investigated size range of 1.6 to 3 μm as indicated in the subsection on boundary and initial conditions.

Table 4. Ratio of passenger exposure to the airborne expiratory particles between the climb and steady level flight legs as an average over the whole cabin volume.

Particle diameter (μm)	Overall cabin passenger exposure ratio between climb and steady level flight legs
2.5	2.2:1
7.5	1.5:1
10	0.2:1

Conclusions and future work

In the current study, airflow design and source control strategies were investigated for their potential to reduce cough-released airborne contaminant exposure in the cabin of a passenger aircraft (Boeing 767-300) during the climb leg. Sulfur hexafluoride (SF_6) was used to mimic the airborne contaminant in the cabin, representing cough-released particles in the size range from 1.6 to 3 μm in diameter. The SF_6 dispersion behavior was analyzed by calculating the concentration time series at two monitoring locations in the cabin, seats A7 and C7, in addition to SF_6 concentration contour plots at the breathing level of the occupants. The concentration time series were used to infer the passenger exposure to the contaminant through determining the area under each curve.

The airflow design strategies researched involved altering the supply airflow direction and changing the supply airflow rate. The source control strategies employed involved changing the cough direction, varying the cough release velocity or volumetric flow rate, and moving the cougher to different locations in the cabin.

Changing the airflow supply angle from the ceiling only, or α , from 20° to 60° had different effects on the SF_6 dispersion behavior in the cabin. The angle $\alpha = 30^\circ$ led to the lowest passenger exposure. However, the 20° and 60° angles, compared to passenger exposure of the baseline climb case with $\alpha = 0^\circ$, resulted in similar and higher exposures, respectively. Further, when a 3D approach was introduced to the airflow redirection scenario through the angle β , directing the airflow to the back of the cabin proved to be better than directing it to the front.

The supply airflow rate to the cabin was changed from the baseline 200 L s^{-1} case to 100% increase, 50% increase, and 50% decrease. As expected, the 100% more airflow scenario led to the highest reduction in passenger exposure locally at the two monitoring points, preceded by the 50% more flow rate. The 50% less airflow rate was not desirable because it increased exposure. However, cabin-wide, increasing the airflow rate by 100% enhanced the contaminant spread as much as the 50% decrease did. From other practical considerations, the energy consumption required for the 100% increase case was significantly higher than that of other cases. For all of these reasons, raising the supply airflow by 50% was found to be the optimal scenario during climb.

For the source control strategies, altering the cough direction was effective in reducing the exposure of the passengers to the released contaminant. This is true when the cough

was directed downwards at either 30° or 40° from the horizontal direction, although no significant difference in exposure alleviation was noticed between the two angles for the same cough orientation. Conversely, directing the cough upwards contributed to increasing the exposure over that for the baseline climb case with a zero angle. This difference in the created exposure between the downwards and upwards cough orientations can be attributed to the ability of the surrounding surfaces and floor to absorb the released contaminant and block its dispersion for the downwards orientation.

Varying the cough release velocity or volumetric rate was achieved in this study in two ways: changing the cough release velocity without fixing the contaminant mass and changing the cough release velocity while keeping the contaminant mass fixed. Adopting the first approach, and on a local level at the two monitoring points, the higher cough velocity of 20 m s^{-1} led to reduced exposure than the lower velocity of 5 m s^{-1} . Nevertheless, cabin-wide, the contaminant dispersion behavior did not show a clear trend, and neither of the two cough velocities clearly resulted in a better air quality condition. For the fixed contaminant mass approach, however, the produced exposure at the two monitoring locations was unrealistically low. This was because the cough released in 0.5 s instead of 1 s lacked the required impulse to propagate throughout the cabin space and was too weak to penetrate the strong airflow currents efficiently.

Relocating the cougher to other locations in the cabin other than the original back row center seat position had a quantifiable effect on the dispersion behavior of the contaminant and, consequently, the exposure. Moving the cougher to the left side of the cabin in the center row (LC location) led to decreased passenger exposure both locally at the monitoring locations and as an average in the whole cabin. On the other hand, moving the cougher to the right side of the cabin in the front row (RF location) caused a substantial increase in the exposure at seat A7, because it is very close to it, whereas it halved the exposure at seat C7. In addition to the proximity of the cougher to specific passengers, the airflow patterns in the cabin, the body forces on the aircraft during climb, and the existence of walls and/or surfaces near the cougher all have confounding effects on the resulted contaminant dispersion behavior from different cougher locations.

Generally, the cases that showed most promising reductions in passenger exposure as an average between the two monitoring locations at seats A7 and C7 with respect to the baseline climb case are the left side center row relocation of the cougher, the $\alpha = 30^\circ$ airflow direction, and the 50% more airflow rate. The exposure ratios are 0.7:1 at seat A7 and 0.5:1 at seat C7 for the first case, 0.7:1 at seat A7 and 0.5:1 at seat C7 for the second case, and 0.6:1 at seat A7 and 0.7:1 at seat C7 for the third case. On the other hand, the highest exposure on average between the two seats occurred for the $\alpha = 60^\circ$ airflow direction case, with 3.5:1 at seat A7 and 2.1:1 at seat C7.

Changing the cough to continuous mouth breathing (exhalation) led to an altered contaminant dispersion behavior in the cabin. For the steady level flight leg, the concentration of the contaminant in the cabin was usually higher

than that during the climb leg. This was attributed to the well-mixed cabin condition created throughout the steady flight leg. As a result, the contaminant concentration increased substantially everywhere in the cabin as opposed to the lower concentrations noticed during the climb leg due to the absence of enough contaminant mixing in the cabin air. The passenger exposure to the contaminant released from the continuous exhalation in the cabin between the climb and steady flight legs was estimated at seats A7 and C7 to be 0.7:1 and 0.9:1, respectively.

Lastly, particles of different sizes were injected in the cabin to represent the expiratory contaminant released from the cough instead of the SF₆ gas. Three particle diameters were used, namely, 2.5 µm representing the fine airborne particles and 7.5 and 10 µm for the coarse particles. The 7.5-µm particles exhibited a combined characteristic between the 2.5- and 10-µm particles. They could remain for long time in the cabin without settling and/or depositing on surfaces. The residence time for the 7.5-µm particles was not noticeably affected by the change in body forces between the climb and steady flight legs, which indicates that this intermediate airborne particle size can pose the greatest infection risk to passengers throughout most of the flight duration.

For future work, and to generalize the findings of the current study, similar parametric analyses need to be implemented on other models of passenger aircraft with different cabin configurations. Moreover, different ventilation strategies, other than the conventional mixing ventilation used in this study, such as underfloor and personalized ventilation systems, can be implemented. Additionally, further combinations and/or additions to the proposed airflow design and source control strategies in the current work can be investigated for possible enhancements in the in-cabin air quality. Finally, investigations on the infection mechanisms using different pathogens, such as influenza, tuberculosis, and severe acute respiratory syndrome (SARS), need to be performed using CFD simulations backed by experimental outbreak data available in the epidemiology literature for specific aircraft cabin models. For those models, the spatial and temporal infection risk of the mentioned diseases can be assessed. In addition, the viability and infectivity of specific pathogens can be imbedded in the simulated models by investigating the influence of environmental factors in the cabin, such as temperature and relative humidity, on the survivability of dispersed pathogens in the cabin space (Aliabadi et al. 2011). It is concluded that multiple detailed investigations related to the influence of aircraft acceleration-induced body forces on ventilation performance of aircraft, an issue that has been neglected in the literature for a long time, are necessary.

ORCID

Hossam A. Elmaghaby  <http://orcid.org/0000-0002-8613-6958>

Yi Wai Chiang  <http://orcid.org/0000-0002-7798-9166>

Amir Abbas Aliabadi  <http://orcid.org/0000-0002-1002-7536>

References

- Airliners. 2017. *Aircraft Technical Data & Specifications/Boeing 767–300*. <https://www.airliners.net/aircraft-data/boeing-767-300/104> (accessed May 9, 2017).
- Aliabadi, A.A. 2018. *Theory and Applications of Turbulence: A Fundamental Approach for Scientists and Engineers*. Guelph, ON, Canada: Amir Abbas Aliabadi Publications.
- Aliabadi, A.A., E.S. Krayenhoff, N. Nazarian, L.W. Chew, P.R. Armstrong, A. Afshari, and L.K. Norford. 2017. Effects of roof-edge roughness on air temperature and pollutant concentration in urban canyons. *Boundary-Layer Meteorology* 164(2):249–79.
- Aliabadi, A.A., S.N. Rogak, K.H. Bartlett, and S.I. Green. 2011. Preventing airborne disease transmission: Review of methods for ventilation design in health care facilities. *Advances in Preventive Medicine* 2011:1–21.
- ANSYS Inc. 2015. *ANSYS Fluent Theory Guide: Release 16.2*. Canonsburg, PA: SAS IP, Inc.
- ASHRAE. 2013. *Standard 161-2013: Air Quality within Commercial Aircraft*. Atlanta: ASHRAE.
- Chang, J.C., and S.R. Hanna. 2004. Air quality model performance evaluation. *Meteorology and Atmospheric Physics* 87(1–3): 167–96.
- Dechow, M., H. Sohn, and J. Steinhanses. 1997. Concentrations of selected contaminants in cabin air of Airbus aircrafts. *Chemosphere* 35:21–31.
- Drake, J.W., and D.E. Johnson. 1990. Measurements of certain environmental tobacco smoke components on long-range flights. *Aviation, Space, and Environmental Medicine* 61(6):531–42.
- Elmaghraby, H.A., Y.W. Chiang, and A.A. Aliabadi. 2018. Ventilation strategies and air quality management in passenger aircraft cabins: A review of experimental approaches and numerical simulations. *Science and Technology for the Built Environment* 24(2):160–75.
- Elmaghraby, H.A., Y.W. Chiang, and A.A. Aliabadi. 2019. Are aircraft acceleration-induced body forces effective on contaminant dispersion in passenger aircraft cabins? *Science and Technology for the Built Environment* (accepted). DOI: 10.1080/23744731.2019.1576457.
- European Centre for Disease Prevention and Control (ECDC). 2018. *Infectious Diseases on Aircraft*. <https://ecdc.europa.eu/en/all-topics-ztravellers-health/infectious-diseases-aircraft> (accessed November 20, 2018).
- Faulkner, W.B., F. Memarzadeh, G. Riskowski, A. Kalbasi, and A.C.-Z. Chang. 2015. Effects of air exchange rate, particle size and injection place on particle concentrations within a reduced-scale room. *Building and Environment* 92:246–55.
- Gudmundsson, S. 2013. *General Aviation Aircraft Design: Applied Methods and Procedures*. Oxford: Butterworth-Heinemann.
- Gupta, J.K., C.-H. Lin, and Q. Chen. 2009. Flow dynamics and characterization of a cough. *Indoor Air* 19(6):517–25.
- Gupta, J.K., C.-H. Lin, and Q. Chen. 2010. Characterizing exhaled airflow from breathing and talking. *Indoor Air* 20(1):31–39.
- Gupta, J.K., C.-H. Lin, and Q. Chen. 2012. Risk assessment of airborne infectious diseases in aircraft cabins. *Indoor Air* 22(5): 388–95.
- Haghighat, F., F. Allard, A.C. Megri, P. Blondeau, and R. Shimotakahara. 1999. Measurement of thermal comfort and indoor air quality aboard 43 flights on commercial airlines. *Indoor and Built Environment* 8(1):58–66.
- Hanna, S.R. 1989. Confidence limits for air quality model evaluations, as estimated by bootstrap and jackknife resampling methods. *Atmospheric Environment* 23(6):1385–98.
- Hanna, S.R., and J. Chang. 2012. Acceptance criteria for urban dispersion model evaluation. *Meteorology and Atmospheric Physics* 116(3–4):133–46.
- Hocking, M.B. 2000. Passenger aircraft cabin air quality: Trends, effects, societal costs, proposals. *Chemosphere* 41(4):603–15.

- Hull, D.G. 2007. *Fundamentals of Airplane Flight Mechanics. Fundamentals of Airplane Flight Mechanics*. New York: Springer.
- Isukapalli, S.S., S. Mazumdar, P. George, B. Wei, B. Jones, and C.P. Weisel. 2013. Computational fluid dynamics modeling of transport and deposition of pesticides in an aircraft cabin. *Atmospheric Environment* 68:198–207.
- Li, F., J. Liu, J. Pei, C.H. Lin, and Q. Chen. 2014. Experimental study of gaseous and particulate contaminants distribution in an aircraft cabin. *Atmospheric Environment* 85:223–33.
- Li, F., J. Liu, J. Ren, X. Cao, and Y. Zhu. 2016. Numerical investigation of airborne contaminant transport under different vortex structures in the aircraft cabin. *International Journal of Heat and Mass Transfer* 96:287–95.
- Lin, C.-H., K.H. Dunn, R.H. Horstman, J.L. Topmiller, M.F. Ahlers, J.S. Bennett, L.M. Sedgwick, and S. Wirogo. 2005. Numerical simulation of airflow and airborne pathogen transport in aircraft cabins—Part I: Numerical simulation of the flow field. *ASHRAE Transactions* 111(1):755–64.
- Mangili, A., and M.A. Gendreau. 2005. Transmission of infections during commercial air travel. *Lancet* 365(9478):2176–77.
- Memarzadeh, F. 2009. Effect of reducing ventilation rate on indoor air quality and energy cost in laboratories. *Journal of Chemical Health and Safety* 16(5):20–26.
- Milton, D.K., M.P. Fabian, B.J. Cowling, M.L. Grantham, and J.J. McDevitt. 2013. Influenza virus aerosols in human exhaled breath: Particle size, culturability, and effect of surgical masks. *PLoS Pathogens* 9(3):e1003205.
- Nagda, N.L., and M. Hodgson. 2001. Low relative humidity and aircraft cabin air quality. *Indoor Air* 11(3):200–214.
- National Aeronautics and Space Administration (NASA). 2015. Forces in a climb. <https://www.grc.nasa.gov/www/k-12/airplane/climb.html> (accessed October 10, 2017).
- Poussou, S.B., S. Mazumdar, M.W. Plesniak, P.E. Sojka, and Q. Chen. 2010. Flow and contaminant transport in an airliner cabin induced by a moving body: Model experiments and CFD predictions. *Atmospheric Environment* 44(24):2830–39.
- Riley, E.C., G. Murphy, and R.L. Riley. 1978. Airborne spread of measles in a suburban elementary school. *American Journal of Epidemiology* 107(5):421–32.
- Strøm-Tejse, P., D.P. Wyon, L. Lagercrantz, and L. Fang. 2007. Passenger evaluation of the optimum balance between fresh air supply and humidity from 7-h exposures in a simulated aircraft cabin. *Indoor Air* 17(2):92–108.
- Sze To, G.N., and C.Y.H. Chao. 2010. Review and comparison between the Wells-Riley and dose-response approaches to risk assessment of infectious respiratory diseases. *Indoor Air* 20(1):2–16.
- Sze To, G.N., M.P. Wan, C.Y.H. Chao, L. Fang, and A. Melikov. 2009. Experimental study of dispersion and deposition of expiratory aerosols in aircraft cabins and impact on infectious disease transmission. *Aerosol Science and Technology* 43(5):466–85.
- Tang, J.W., A.D. Nicolle, C.A. Klettner, J. Pantelic, L. Wang, A. Bin Suhaimi, A.Y.L. Tan, G.W.X. Ong, R. Su, C. Sekhar, D.D.W. Cheong, and K.W. Tham. 2013. Airflow dynamics of human jets: sneezing and breathing—Potential sources of infectious aerosols. *PLoS One* 8(4):e59970.
- University of Southampton. 2005. *Weight, Geometry, Lift, Drag and Thrust Properties*. [http://www.southampton.ac.uk/~jps7/Aircraft Design Resources/Sydney aerodynamics for students/perf/perf_ac.html](http://www.southampton.ac.uk/~jps7/Aircraft%20Design%20Resources/Sydney%20aerodynamics%20for%20students/perf/perf_ac.html) (accessed May 10, 2017).
- Wan, M.P., G.N. Sze To, C.Y.H. Chao, L. Fang, and A. Melikov. 2009. Modeling the fate of expiratory aerosols and the associated infection risk in an aircraft cabin environment. *Aerosol Science and Technology* 43(4):322–43.
- Waters, M.A., T.F. Bloom, B. Grajewski, and J. Deddens. 2002. *Measurements of indoor air quality on commercial transport*

aircraft. *Proceedings of the 9th International Conference on Indoor Air Quality and Climate*. Monterey, CA, June 30–July 5, pp. 782–87.

- Yan, J., M. Grantham, J. Pantelic, D.K. Milton, F. Liu, S. Ehrman, P.J. Bueno de Mesquita, and B. Albert. 2018. Infectious virus in exhaled breath of symptomatic seasonal influenza cases from a college community. *Proceedings of the National Academy of Sciences* 115(5):1081–86.
- Yang, L., X. Li, Y. Yan, and J. Tu. 2018. Effects of cough-jet on airflow and contaminant transport in an airliner cabin section. *The Journal of Computational Multiphase Flows* 10(2):72–82.
- Zhang, Z., X. Chen, S. Mazumdar, T. Zhang, and Q. Chen. 2009. Experimental and numerical investigation of airflow and contaminant transport in an airliner cabin mockup. *Building and Environment* 44(1):85–94.

Appendix: Procedure for determining the aircraft acceleration components during the climb leg

Newton's second law is applied on the vertical and horizontal axes shown in Figure A1:

$$\sum \vec{F} = m\vec{a}. \quad (\text{A1})$$

On the vertical axis:

$$T\sin\theta - D\sin\theta + L\cos\theta - W = m\vec{a}_v, \quad (\text{A2})$$

and on the horizontal axis:

$$T\cos\theta - D\cos\theta - L\sin\theta = m\vec{a}_h, \quad (\text{A3})$$

where \vec{a}_v and \vec{a}_h are the vertical and horizontal acceleration components, respectively (Gudmundsson 2013).

The unknowns (T , θ , D , L , m) were estimated based on industrial specifications and dimensions for the Boeing 767-300 aircraft (Airliners 2017):

$T = 462.6 \text{ kN}$ (for a twin-jet engine), $\theta = 20^\circ$, $m = 159,210 \text{ kg}$ (max. takeoff weight), and $W = mg$.

$$D = C_D * 0.5\rho V^2 A, \quad (\text{A4})$$

$$L = C_L * 0.5\rho V^2 A, \quad (\text{A5})$$

where C_D and C_L are the drag and lift coefficients, respectively; ρ is the air density; V is the aircraft velocity (taken as 155 m s^{-1}); and A is the reference (wing) area. The drag coefficient is given as

$$C_D = C_{D0} + kC_L^2, \quad (\text{A6})$$

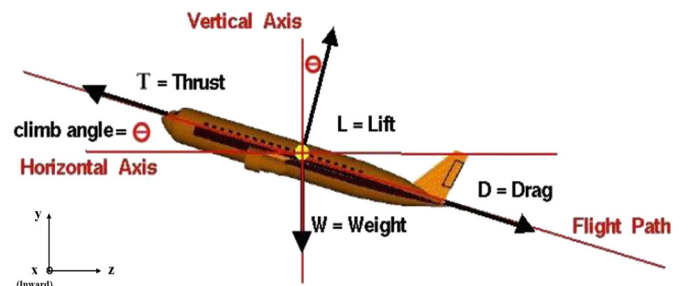


Fig. A1. Forces on a passenger aircraft during climb with the two axes (horizontal and vertical) set for the calculation of acceleration components.

C_{D_0} is the part of drag coefficient due to friction and pressure on the aircraft body, and K is a constant that incorporates the other part of the drag coefficient due to lift (lift induced drag) (University of Southampton 2005). $C_D = 0.06$ (approximation for many aircraft aerofoils). The constant is

$$k = \frac{1}{\pi AR e}, \quad (\text{A7})$$

where e is equal to 0.85 for twin-engine wide-body aircraft, and AR is the wing aspect ratio, which is determined from

$$AR = \frac{(\text{wing span})^2}{\text{wing area}} = \frac{(47.57)^2}{283.3} = 7.987. \quad (\text{A8})$$

These yield $k = 0.04688$. Taking $C_{D_0} = 0.017$ for a twin-engine wide-body and substituting in Equation A6 yields $C_L = 0.96$. Substituting in Equations A4 and A5 and assuming the density of atmospheric air to be 1.2 kg m^{-3} ,

$$D = 229.473 \text{ KN},$$

and

$$L = 3671.568 \text{ KN}.$$

Substituting in Equations A2 and A3, the vertical and horizontal components of the aircraft acceleration are, respectively,

$$\vec{a}_v = 13.79 \text{ ms}^{-2} = -1.4 \vec{g},$$

and

$$\vec{a}_h = -6.51 \text{ ms}^{-2} = 0.67 \vec{g}.$$

Lastly, the absolute acceleration components calculated are expressed in the form of relative acceleration components on the air inside the aircraft cabin before being implemented in FLUENT. This is attained by reversing the sign of each acceleration component and superimposing it on any acceleration(s) that may exist in the same direction (e.g., gravity). This is justified by Newton's third law and yields the relative acceleration components as follows:

$$\vec{a}_y = (-13.79 - 9.81) = -23.6 \text{ ms}^{-2} = 2.4 \vec{g},$$

(or 23.6 ms^{-2} acting downwards) and

$$\vec{a}_z = 6.51 \text{ ms}^{-2} = -0.67 \vec{g}.$$

(or 6.51 ms^{-2} acting toward the tail of the aircraft).